Atmos. Chem. Phys. Discuss., 11, 5435–5491, 2011
www.atmos-chem-phys-discuss.net/11/5435/2011/
doi:10.5194/acpd-11-5435-2011

Atmospheric Chemistry and Physics Discussions

Transport of anthropogenic emissions during ARCTAS-A: a climatology and regional case studies

D. L. Harrigan[1,4], H. E. Fuelberg[1], I. J. Simpson[2], D. R. Blake[2], G. R. Carmichael[3], and G. S. Diskin[5]

[1]Department of Meteorology, Florida State University, Tallahassee, FL, USA
[2]Department of Chemistry, University of California, Irvine, CA, USA
[3]Center for Global and Regional Environmental Research, University of Iowa, Iowa City, IA, USA
[4]National Oceanic and Atmospheric Administration, National Weather Service, Tallahassee, FL, USA
[5]NASA Langley Research Center, Hampton, VA, USA

Received: 12 January 2011 – Accepted: 31 January 2011 – Published: 15 February 2011

Correspondence to: H. E. Fuelberg (hfuelberg@fsu.edu)

Published by Copernicus Publications on behalf of the European Geosciences Union.

Abstract

The National Aeronautics and Space Administration (NASA) conducted the Arctic Research of the Composition of the Troposphere from Aircraft and Satellites (ARCTAS) mission during 2008 as a part of the International Polar Year (IPY). The purpose of ARCTAS was to study the factors responsible for changes in the Arctic's atmospheric composition and climate. A major emphasis was to investigate Arctic haze, which is most pronounced during winter and early spring. This study focuses on the spring phase of ARCTAS (ARCTAS-A) that was based in Alaska during April 2008. Although anthropogenic emissions historically have been associated with Arctic haze, biomass burning dominated the ARCTAS-A period and has been the focus of many ARCTAS related studies.

This study determines the common pathways for anthropogenic emissions during ARCTAS-A. Trajectories (air parcels) are released each day from three historically significant regions of anthropogenic emissions (Asia, North America, and Europe). These fifteen day forward trajectories are calculated using data from the Weather Research and Forecasting (WRF) model at 45 km horizontal resolution. The trajectories then are examined to determine: origins of emissions that reach the Arctic (defined as north of 70° N) within fifteen days, pathways of the emissions reaching the Arctic, Arctic entry locations, and altitudes at which the trajectories enter the Arctic. These results serve as regional "climatologies" for the ARCTAS-A period.

Three cases during the ARCTAS-A period (one for each of the regions above) are examined using backward trajectories and chemical fingerprinting based on in situ data sampled from the NASA DC-8. The fingerprinting utilizes volatile organic compounds that represent pure anthropogenic tracers, Asian anthropogenic pollution, incomplete combustion, and natural gas emissions. We determine flight legs containing anthropogenic emissions and the pathways travelled by these emissions. Results show that the DC-8 sampled anthropogenic emissions from Asia, North America, and Europe during the spring phase of ARCTAS. The pathways travelled by these emissions agree

ACPD

11, 5435–5491, 2011

with our derived "climatologies" and previous studies of Arctic transport. Meteorological analysis and trajectory calculations indicate that middle latitude cyclones and their associated warm conveyor belts play an important role in lofting the surface based emissions to their sampling altitude in all three cases.

1 Introduction

Since the Arctic is far removed from most industrial locations and other sources of pollution, its atmosphere long was believed to be very clean (Stohl, 2006; Law and Stohl, 2007). However, parts of the Arctic actually can become very polluted due to the transport of emissions from distant sources (Raatz and Shaw, 1984; Shaw, 1995; Rinke et al., 2004). The greatest concentrations of Arctic pollution occur during the winter and early spring months (Mitchell, 1957; Shaw, 1995; Eckhardt et al., 2003). The buildup of pollutants during these months, combined with photochemical reactions (beginning in early spring), produce a visibility reducing haze called "Arctic Haze" (Mitchell, 1957; Shaw, 1983; Hileman, 1983; Schnell, 1984; Meyer et al., 1990). This phenomenon first was documented during the 1950's by Air Force pilots during weather reconnaissance flights (Mitchell, 1957). The haze typically is most concentrated near the surface, with discontinuous horizontal layers in the middle and upper troposphere (Hileman, 1983; Hoff, 1987).

Arctic haze long was considered to consist mostly of anthropogenic pollutants (Hileman, 1983; Barrie and Hoff, 1985; Barrie et al., 1994; Stohl, 2006; Warneke et al., 2009), with primary species being a mixture of sulphates and particulate organic matter (Li and Barrie, 1993; Quinn et al., 2002). Other species include ammonium, nitrate, dust and black carbon (Li and Barrie, 1993; Quinn et al., 2002). Shaw (1995) noted that heavy metals detected in the haze are associated with industrial sources. Recent research has shown that boreal forest fires in Siberia and Eastern China, as well as agricultural burning in Kazakhstan, Southern Russia, and Eastern Europe also are important sources of Arctic pollution (Warneke et al., 2009, 2010). This source of

ACPD
11, 5435–5491, 2011

biomass emissions may increase in the future due to the effects of climate change (e.g., Kasischke et al., 2005; Wotton et al., 2010).

Several factors contribute to the buildup of pollutants in the Arctic atmosphere. First, the Arctic atmosphere is dominated by strong temperature inversions that trap air near the surface, especially during the winter and early spring when there is little or no sunlight (Curry, 1983, 1987; Raatz, 1991; Bradley et al., 1992). Since these inversions limit turbulent mixing, dry deposition also is greatly reduced (Hileman, 1983; Stohl and Law, 2006). Furthermore, since the atmosphere during the winter and early spring is cold, dry, and stable, precipitating cloud systems are inhibited, thereby limiting wet deposition (Shaw, 1995). Another phenomenon that influences cold season Arctic transport is the "dome" of cold potential temperature that forms over the polar region (Klonecki et al., 2003; Stohl, 2006; Law and Stohl, 2007). Since potential temperature increases with altitude in the stable atmosphere, and due to the temperature difference between the middle latitudes and the Arctic, the potential temperature (isentropic) surfaces curve upward from the mid latitudes to the Arctic (Carlson, 1981; Iverson, 1984; Raatz, 1991). If one assumes adiabatic conditions, low level air parcels moving northward from the middle latitudes must ascend as they approach the Arctic. Conversely, for parcels to remain near the surface, they must be diabatically cooled by radiative effects or other processes during passage over the ice covered surfaces.

Three typical transport pathways to the Arctic during the winter months have been identified by Stohl (2006) and Stohl and Law (2006). The first consists of rapid low level transport of already cold air north of the Arctic front. A variation of this scenario is rapid transport of air that is lifted over the Arctic front. The second method of transport occurs on a longer time scale in which cold air is transported over a snow covered surface, allowing it to cool sufficiently to penetrate the Arctic isentropic dome. Finally, middle latitude air can be lofted into the upper troposphere and then quickly transported to the Arctic where it gradually sinks into the lower troposphere due to radiative cooling. These three transport processes generally mean that European emissions are the dominant source of pollutants in the low levels of the Arctic atmosphere, while North

ACPD
11, 5435–5491, 2011

American and East Asian pollutants are more common in the middle and upper levels (Klonecki et al., 2003; Stohl, 2006; Law and Stohl, 2007).

The National Aeronautics and Space Administration (NASA) conducted the Arctic Research of the Composition of the Troposphere from Aircraft and Satellites (ARCTAS) field mission during 2008 (Jacob et al., 2010). ARCTAS was conducted primarily over the Arctic areas of Alaska, Canada, and Greenland and was a component of the Polar Study using Aircraft, Remote Sensing, Surface Measurements and Models of Climate, Chemistry, Aerosols and Transport (POLARCAT, Stohl and Law, 2006). ARCTAS consisted of two deployments, one based in Alaska (April 2008) and the other in Alberta, Canada (June–July 2008) (Jacob et al., 2010). The main goal of ARCTAS was to better understand the factors that contribute to changes in the composition of the Arctic atmosphere and climate by studying the influx of mid-latitude pollutants, boreal forest fire emissions, aerosol radiative forcing, and chemical processes (Jacob et al., 2010).

Anthropogenic emissions were expected to dominate the Arctic atmosphere during the spring phase of ARCTAS (hereafter denoted ARCTAS-A). However, that did not occur. Instead, widespread fires in Russia were the major source of Arctic pollution during the period (Warneke et al., 2009; Jacob et al., 2010). The fires started unusually early, consisting of agricultural burning in Kazakhstan and Southern Russia as well as boreal forest fires in Siberia (Warneke et al., 2009). ARCTAS related research has examined the sources and characteristics of the biomass emissions (e.g., Kondo et al., 2010; Matsui et al., 2010; Oltmans et al., 2010; Singh et al., 2010). Although biomass burning emissions were the dominant source of Arctic pollution during ARCTAS-A, our focus is the characteristics and transport pathways of anthropogenic emissions during the spring period, specifically the influx of mid-latitude anthropogenic pollutants to the Arctic and how the transport pathways during the spring (April) phase of ARCTAS compare with those previously described in the literature. We utilize in situ chemical data sampled from the NASA DC-8 flying laboratory and backward kinematic trajectories derived from high resolution numerical modeling to identify source regions of the

ACPD
11, 5435–5491, 2011

anthropogenic emissions that were sampled by the aircraft. Three specific cases are examined, one for each of the major source regions (Europe, Asia, and North America). These cases are compared to transport occurring during the entire spring phase of ARCTAS.

Section 2 provides details about the meteorological numerical model that we employed as well as the trajectory products derived from its output. Information about other methodologies and the specifics of our various data sources also is provided. Sections 3–8 present derived ARCTAS-A "climatologies" for each of the three major source regions as well as results from the three cases of anthropogenic Arctic transport.

2 Data and methodology

2.1 WRF model

Numerical simulations were used to study weather patterns responsible for transport to the Arctic (defined as the region north of 70° N) during the ARCTAS mission. This study utilized the Weather Research and Forecast (WRF) model (Skamarock et al., 2008) version 3.0.1.1 developed by the National Center for Atmospheric Research (NCAR). The parent domain had a 45 km horizontal resolution centered on the North Pole (Fig. 1). Inner telescoping nests of 15 and 5 km were centered over three historically significant anthropogenic source regions including Europe, Eastern Asia, and North America. These inner nests provided two-way feedback to the coarse grid. The parent domain and each of the inner nests consisted of 50 vertical sigma levels that were packed in the boundary layer and near the tropopause. The specific physics packages used in our WRF simulations are listed in Table 1 and Fuelberg et al. (2010). In depth discussions about each of the settings in Table 1 can be found in Skamarock et al. (2008). The model was initialized with final analysis data from the Global Forecast System (GFS) at 0.5° × 0.5° horizontal resolution. GFS

ACPD
11, 5435–5491, 2011

is run operationally by the National Center for Environmental Prediction (available at http://www.nco.ncep.noaa.gov/pmb/products/).

2.2 Trajectory calculations

Trajectories were calculated using hourly wind data from the WRF 45 km grid. Trajectories represent the paths taken by air parcels over a period of time. Specific information on the trajectory model can be found in Fuelberg et al. (1996, 2000) and Martin et al. (2002). Limitations of trajectories are described in Stohl et al. (1995, 1998) and Fuelberg et al. (2000). Although Lagrangian particle dispersion models have some advantages over trajectories, trajectories were more appropriate for the applications that are described in the following paragraphs. We used trajectories to (1) derive general transport statistics for the three regions of interest (Europe, Asia, and North America) during the entire ARCTAS-A period, and (2) to study transport during three specific case studies (one for each region listed above).

Anthropogenic CO emissions data from the University of Iowa Center for Global and Regional Environmental Research (CGRER) were used to define trajectory "release" locations in regions of emissions (Fig. 2). These data had been prepared to support the ARCTAS mission (for further information and data access, see http://www.cgrer.uiowa.edu/arctas/emission.html).

To derive general transport statistics during ARCTAS-A, fifteen day forward trajectories (air parcels) were released at the surface on a $2.0^{\circ} \times 2.0^{\circ}$ grid within the domains of each of our areas of interest. Releases were made each day (~ 02:00 p.m. LDT) during the period 19 March through 17 April 2008, with data for the final day of trajectories extending to 3 May 2008.

Trajectories for the three case studies were calculated using the same trajectory model described above and using the same WRF-derived wind data. The trajectories (air parcels) were released at 1 min intervals along specific legs of DC-8 flights 5 and 8 (Fig. 3) and extended 15 days backward in time.

ACPD
11, 5435–5491, 2011

2.3 Chemical data

Chemical species data used in this study were collected by two groups aboard the NASA DC-8 during the ARCTAS campaign. The University of California-Irvine (UCI) atmospheric chemistry group used whole air sampling (WAS) techniques to measure 76 speciated volatile organic compounds (VOCs)(Simpson et al., 2010), and NASA Langley used the DACOM instrument to measure methane (CH_4) and carbon monoxide (CO) (Sachse et al., 1987; Anderson et al., 1996, Blake et al., 1996). We used these data to identify anthropogenic emissions and tag their respective source regions. In particular we used carbonyl sulphide (OCS), halon-1211 (H-1211), methyl chloride (CH_3Cl) and 1,2-dichlorethene (1,2-DCE) as tracers of Asian anthropogenic pollution plumes (Barletta et al., 2009); ethyne (C_2H_2) and benzene (C_6H_6) as tracers of incomplete combustion, including biomass burning and/or urban fossil fuel (Blake et al., 2003; Warneke et al., 2007); methane (CH_4), ethane (C_2H_6) and propane (C_3H_8) as probes for natural gas (Katzenstein et al., 2003; Xiao et al., 2008); and tetrachloroethene (C_2Cl_4) and HCFC-22 as purely anthropogenic tracers since they have no known natural sources (Aucott et al., 1999; Simpson et al., 2004).

Measurements of CO and CH_4 using the DACOM diode laser absorption instrument were made with 1 s temporal resolution during the entire ARCTAS campaign, except for brief periodic calibration intervals. The DACOM measurements were averaged to the sampling period of the WAS instrument for this study. Details about the DACOM instrument may be found in Sachse (1987, 1988). Specific information about the WAS sampling techniques and processing of these data can be found in Blake (2008), Simpson et al. (2010), and the references therein. Briefly, 168 whole air canisters were loaded on the DC-8 prior to each flight, and were filled sequentially throughout the flight. Sampling times typically were 1 min during horizontal flight legs, and 30 s to 1 min during ascents and descents. Because of the finite number of canisters, samples generally were taken every 4–5 min, and more frequently during ascents, descents, and plume encounters. The detection limit, precision and accuracy of the measurements vary

ACPD
11, 5435–5491, 2011

by compound, and are shown for the 10 species that we considered in Tables 2–4 of the results section. These 10 compounds have a range of atmospheric lifetimes, from 9 days (benzene) to 16 years (H-1211) (Tables 2–4). Since trace gases undergo chemistry and mixing as soon as they are released from their emission source, a short-lived gas such as benzene will become relatively more depleted during its multi-day transit from its emission source to the DC-8 sampling location. Therefore, our identification of anthropogenic plumes from specific emission source regions was based on a combination of chemical fingerprinting and back trajectory analysis, rather than by attempting to compare the measured data to known emission ratios from specific sources, which requires relatively fresh plumes to be sampled (minutes to hours old).

An additional consideration in the analysis is that many of the trace gases being examined vary with time (diurnally, seasonally, and annually) and space (latitudinally and altitudinally). For example HCFC-22 is experiencing rapid year-to-year growth (Montzka et al., 2009), whereas global C_2Cl_4 levels are continuing a long-term decline (Simpson et al., 2004). Therefore, we calculated a local background for each compound that is appropriate for the season and latitudes that were sampled during ARCTAS-A. Specifically, data from DC-8 flights 4–10 were used (this excludes flights 3 and 11, which were transit flights between Palmdale, CA and Fairbanks, AK). Stratospheric data were removed by choosing a cutoff of $O_3 > 100$ ppbv. Furthermore, O_3 depletion episodes at low altitudes were removed by choosing a cutoff of $O_3 < 45$ ppbv. These criteria removed 338 of 1126 data points, leaving 788 points. The background average for each compound then was calculated using the lowest quartile (25%) of the remaining data ($n = 197$). These local background averages were compared to the plume enhancements.

3 Eastern Asian transport during ARCTAS-A

To identify the Arctic bound transport pathways specific to Eastern Asia (as defined Fig. 2a), 15 day forward trajectories were calculated from the WRF model data. During

ACPD
11, 5435–5491, 2011

the period 19 March through 17 April 2008, trajectories (air parcels) were launched each day from the 173 grid points in the Asian domain (Fig. 2a), producing a total of 5363 releases during the 31 day period. After the trajectories were calculated, their information was combined to determine (1) the number of trajectories (per release grid point) that reached the Arctic (crossed 70° N) within the 15 day period; (2) the common pathways taken by these trajectories; (3) common Arctic entry locations along the 70° N latitude belt; (4) and the pressure level at which the trajectories entered the Arctic.

Figure 4a shows the origins of Asian trajectories that enter the Arctic during ARCTAS-A. In general, trajectories released farther north have a greater chance of being transported to the Arctic within 15 days, while some locations in the southern portion of the domain fail to produce any Arctic bound trajectories. Within the Asian domain, 40.2% of the 528 Arctic bound trajectories were released at a latitude greater than 40° N, 54.7% came from the region between 30° N and 40° N, and only 5.1% originated further south than 30° N.

To determine the pathways taken by trajectories crossing 70° N, the hourly position of each trajectory that reached the Arctic was plotted (Fig. 4b shows the results at 1° × 1° resolution). Once a trajectory entered the Arctic, it was no longer tracked. In addition, if a trajectory exited the Arctic and subsequently re-entered, only the first entrance was recorded. Although the plot shows trajectory counts at each grid point, it clearly depicts high traffic regions that can be interpreted as pathways. Most trajectories released from Asia travel eastward, and one distinct pathway is evident. It extends across Eastern Siberia and the North Pacific Ocean, over the Bering Sea, northward across Western Alaska, and into the Arctic. Other "hot spots" are located across Western Canada and the Central United States.

The aforementioned primary pathway is reflected in the plot of Arctic entry locations (Fig. 4c), where each colored circle represents an entry region that is 5° longitude wide. The most common Arctic entry location from Eastern Asia is along the extreme northeastern part of Siberia, eastward through the Chukchi Sea, and along Northwestern and North-Central Alaska. In fact, 61.5% of the trajectories that reach the Arctic enter

ACPD
11, 5435–5491, 2011

between 180–140° W. Very few Asian trajectories enter the Arctic from the Northeastern Atlantic Ocean and locations eastward through Western and Central Russia.

The most common Arctic arrival pressures for Asian trajectories are in the middle (850–500 hPa) and upper (less than 500 hPa) troposphere (Fig. 4d). Only 3.2% of the trajectories reaching the Arctic do so in the lower troposphere (greater than 850 hPa), while 40.5% arrive in the middle troposphere and 56.3% arrive in the upper troposphere.

4 Eastern Asian case study

We now present an example of Asian anthropogenic transport using chemical tracers sampled by the DC-8 and backward trajectories from these sampling sites. We fingerprint the source region of the sampled anthropogenic emissions and describe its transport pathway and the weather patterns responsible for this transport. Asian emissions have been found to be more efficient in producing tropospheric ozone than European and North American sources (Stohl et al., 2002). Thus, understanding the pathways and receptor regions of Asian anthropogenic emissions is important in understanding atmospheric chemistry budgets of the Arctic.

Leg 5 of DC-8 flight 8 on 12 April 2008 is an example of transport from Asia to the Arctic. Flight legs were determined using standard techniques of the Florida State University (FSU) Meteorology group (more information can be found at http://fuelberg.met.fsu.edu/research/arctas/traj/traj.html). Leg 5 extends between 17:30 and 18:03 UTC, and is shown in Fig. 3b as the southernmost red segment, just south of Nunyak Island, AK.

4.1 Chemical fingerprinting

Asian outflow consists of a complex mixture of industrial, biofuel, and biomass burning emissions (Russo et al., 2003; Streets et al., 2003). Distinguishing anthropogenic

ACPD
11, 5435–5491, 2011

influences from biomass burning during ARCTAS-A is complex since the influence of biomass burning was significant. However, based on airborne measurements made during NASA's Intercontinental Chemical Transport Experiment (INTEX-B), Barletta et al. (2009) noted that China has a distinct anthropogenic chemical fingerprint consisting of enhanced levels of carbonyl sulphide (OCS), methyl chloride (CH_3Cl), 1,2-dichloroethane (1,2-DCE), ethyl chloride, and halon-1211 (H-1211). The following description indicates that the ARCTAS flight 8, leg 5 chemical signature is consistent with that fingerprint.

Carbonyl sulphide has several sources, including oceans, biomass burning, aluminum production, and coal combustion (Watts, 2000; Kettle et al., 2002; Blake et al., 2004). Sources of CH_3Cl include biomass burning and biofuel use, while 1,2-dichloroethane primarily is anthropogenic and is used as a chemical intermediate in synthesizing other compounds (Barletta et al., 2009). Halon-1211, a purely anthropogenic tracer, is used in firefighting (Butler et al., 1998; Fraser et al., 1999). Halon-1211 also contributes to stratospheric ozone depletion, although its global abundance has begun to decline in recent years (http://cdiac.ornl.gov/trends/otheratg/blake/data.html). Although CH_3Cl and OCS can have both anthropogenic and biomass burning sources, their origins can reasonably be classified as anthropogenic when well correlated with H-1211 and 1,2-DCE. These species, as well as tetrachloroethene (C_2Cl_4, an industrial solvent and purely anthropogenic tracer) and HCFC-22 (a refrigerant and purely anthropogenic tracer) (Aucott et al., 1999; Blake et al., 2003) are plotted in Fig. 5 with respect to sampling altitude along DC-8 flight 8 on 12 April 2008.

Sampling altitudes, as well as mixing ratios identify three data points between 7500–8300 m that represent the plume sampled along leg 5. The figure contains six composite plots with leg 5 indicated by the red points. The blue points also denote data from leg 5, specifically the subset of leg 5 data that represents the plume that will be examined. All other legs along flight 8 are represented by the black points.

Figures 5a–d show the tracers described by Barletta et al. (2009) as being an anthropogenic fingerprint for China. It is clear that the data points representing the plume

ACPD
11, 5435–5491, 2011

(blue) are enhanced over the background values for the flight. Furthermore, a relatively strong average correlation ($r^2 = 0.81$) between these four tracers supports the conclusion that OCS and CH_3Cl within the leg 5 plume are of anthropogenic origin. Further strengthening the hypothesis that anthropogenic emissions were sampled along leg 5 is the fact that two purely anthropogenic tracers (C_2Cl_4 and HCFC-22, Figs. 5e,f) are enhanced over background values.

Mean background mixing ratios for each of the species above were determined using data from ARCTAS-A flights 4–10 (as described in Sect. 2.3) and are presented in Table 2. These values are compared with mean mixing ratios in the plume along leg 5. All species listed in Table 2 show higher mixing ratios in the leg 5 Asian plume than in background air measured during ARCTAS-A. The mean values of 1,2-DCE, C_2Cl_4, CH_3Cl, OCS, HCFC-22, and H-1211 in the Asian plume are enhanced by 420, 61, 30, 26, 8 and 7%, respectively, over their mean background values (Table 2). One should note that these relative enhancements generally decrease with increasing atmospheric lifetime of each compound. This is consistent with longer-lived species being more abundant (higher background values) in the atmosphere, therefore producing relatively smaller enhancements.

To summarize, enhancements in three purely anthropogenic tracers (C_2Cl_4, H-1211, and HCFC-22) signal an anthropogenic influence along leg 5 of flight 8 on 12 April 2008. Furthermore, four species known to be specific to Chinese anthropogenic emissions (1,2-DCE, OCS, H-1211, and CH_3Cl) are well correlated along leg 5. The two species that can have either biomass or anthropogenic emissions (OCS and CH_3Cl) are concluded to be of anthropogenic origins since they are well correlated with the remaining two anthropogenic tracers (H-1211 and 1,2-DCE). Furthermore, the anthropogenic signature along leg 5 is enhanced compared to all other flights during ARCTAS-A. Thus, based on chemistry alone, Chinese anthropogenic emissions were sampled along leg 5. This Chinese source is examined from a meteorological perspective in the next section.

ACPD
11, 5435–5491, 2011

4.2 Transport and meteorology

Fifteen day backward trajectories (air parcels) were released at 1 min intervals along flight leg 5 within the 500–300 hPa layer, a total of 34 releases. We monitored whether each trajectory passed into the model-derived boundary layer during its transit, and all 34 trajectories were found to have done so (Fig. 6a). Boundary layer encounters are important since they indicate that surface based emissions are accessed for transport. Figure 6b shows only those segments of the trajectories in Fig. 6a that are in the boundary layer. In combination with the trajectories in Fig. 6a,b, WRF constant pressure analyses are examined to determine the factors contributing to the transport of emissions.

After release from the aircraft, the trajectories split into two branches as they travel backward over the Sea of Okhotsk (Fig. 6a). Branch 1 is the most dispersive, with many trajectories located over Asia 15 days prior to sampling. The paths become more consolidated as the trajectories pass over the Koreas and then make a loop near 35° N, 175° E before heading toward Southern Alaska and the DC-8. Average locations of the trajectories when the boundary layer is encountered are shown in Figs. 6b and 7a, and in Fig. 7b when deep ascent occurs. The number within each red circle of Fig. 7 is the time (in days) prior to the flight encounter. Ten days prior to DC-8 sampling (Fig. 7a), the trajectories are located in the boundary layer over Eastern Asia, just north of the Koreas, where anthropogenic emissions are enhanced (Fig. 2b). The trajectories then move offshore over the Western Pacific to a position south of the Kamchatka Peninsula and follow a looping track for the next five days (Fig. 6a) due to a series of troughs and ridges over the Northwest Pacific. A low pressure system develops off the eastern coast of Japan, strengthens, and moves northward during the final three days of transit (Fig. 7b). The trajectories are located in the warm sector of this middle latitude cyclone where they experience rapid ascent and arrive at the aircraft under the influence of upper level westerly flow.

ACPD
11, 5435–5491, 2011

Branch 2 of the trajectories comprising leg 5 (Fig. 6a) exhibits a more direct route to the DC-8. Figure 8 shows their average locations both when the boundary layer is encountered (Fig. 8a) and when deep ascent occurs (Fig. 8b). Fifteen days prior to aircraft sampling, the trajectories are in the boundary layer over Southern Asia near Bangladesh and Bhutan (Figs. 6b, 8a). Similar to branch 1, this is an area of major anthropogenic emissions (Fig. 2b). The weather pattern is rather benign at this time, and the trajectories take a slow, almost negligible eastward track through the lower troposphere for the next several days (Fig. 8a). At 3 days prior to sampling (Fig. 8b) they are east of Japan in the warm sector of a middle latitude cyclone where they undergo ascent. For the remainder of the time until reaching the aircraft, they are transported northeastward in the upper troposphere.

Figure 6c presents the trajectories from Fig. 6a in a pressure versus time reference frame. Both branches of trajectories experience deep ascent within the 4 days prior to flight 8. The distribution on earlier days is poorly defined due to the different paths taken by the individual trajectories. Synoptic analyses indicate that the strong ascent occurs when the trajectories are within a cyclone's warm sector (Figs. 7b, 8b), suggesting that the ascent may be due to a warm conveyor belt (WCB). A WCB is an airstream ahead of a surface cold front that originates near the surface of a cyclone's warm sector and then ascends to the upper troposphere (e.g., Eckhardt et al., 2004). Warm conveyor belts play an integral role in transporting boundary layer air into the upper levels of the atmosphere where it can undergo subsequent long range transport (Ding et al., 2009). WCBs most commonly originate along the east coasts of North America and Asia and are more frequent during winter than summer (Stohl, 2001; Eckhardt et al., 2004). Based on a 15 year climatology, Eckhardt et al. (2004) determined the timescale of WCBs to be ~ 2 days. They classified "reasonably strong" WCBs based on trajectories that, during a 2 day time period, ascended 60% of the tropopause height and moved eastward at least 10° longitude and northward at least 5° latitude.

We examined each of the leg 5 boundary layer trajectories (Fig. 6a) to determine if they satisfied the "reasonably strong" WCB criteria in Eckhardt et al. (2004). The 2 day

ACPD
11, 5435–5491, 2011

periods were calculated back from each hourly position along the trajectory path. Results show that 100% of the trajectories met the required northward and eastward displacement criteria during a 2 day period. We then determined whether the trajectories' ascent exceeded 60% of the tropopause height as defined by our WRF simulations. Although the tropopause height varies spatially and temporally, its average height in our 30–60° N window (where the ascent occurred) was 10,366 m, agreeing closely with the values in Eckhardt et al. (2004). Sixty percent of the average tropopause height is 6,219 m. Results show that 71% of the trajectories in Fig. 6a ascend at least this amount during a 48 h period.

Eckhardt et al. (2004) noted that most of the moisture at the start of a WCB is converted to precipitation, thereby producing decreased humidity and an increase in potential temperature. The potential temperatures of their trajectories undergoing WCB processes increased 15–22 K within a 48 h period. We calculated the 48 h change in potential temperature along the leg 5 trajectories in Fig. 6a. Fifty-six percent of them satisfy the 15–22 K increase criterion, with 95% of these cases coinciding with ascent greater than 60% of the tropopause height. If we assume that either the horizontal and vertical criteria, or the horizontal and potential temperature criteria must be met for WCB processes to be verified, our percentage increases from 71 to 74%. Although not all of the leg 5 trajectories satisfy each of the Eckhardt et al. (2004) WCB criteria, many do, and all of the trajectories fulfill the horizontal requirements. These results strongly suggest that most of the trajectories in Fig. 6a did experience "reasonably strong" WCB processes as defined by Eckhardt et al. (2004).

In summary, these sections have detailed model-derived transport from Asia, chemical fingerprinting based on in situ aircraft measurements, as well as trajectory and meteorological analyses. The results have shown that chemical tracers specific to Asian and Chinese anthropogenic emissions were sampled during leg 5 of the flight. Trajectory analyses revealed that this air had intersected areas of enhanced anthropogenic emissions across Eastern Asia within the boundary layer (Fig. 2b). The emissions then

ACPD
11, 5435–5491, 2011

were transported eastward from the Asian continent where they most likely underwent WCB related ascent prior to reaching the DC-8 at flight level on 12 April 2008.

5 North American transport during ARCTAS-A

We next examine the transport of North American anthropogenic emissions to the Arctic. Trajectories were released at 178 grid points over North American anthropogenic sources (Fig. 2c,d) each day during ARCTAS-A, producing a total of 5518 releases during the 31 day period. Similar to the Asian domain (Fig. 4a), the distribution of Arctic arrivals favors the northern half of the region (Fig. 9a). Origins at latitudes greater than 40° N produce 47% of the Arctic bound trajectories, while 50% of the trajectories originate between 30–40° N. Only a small percentage (3%) of trajectories originating at latitudes less than 30° N reach the Arctic within 15 days. A close examination of the trajectories crossing 70° N (Fig. 9b), reveals two pathways; one is distinct, and the other less defined. The most distinct pathway transports air north from its release points. This path continues across Northeastern Canada and enters the Arctic over Baffin Bay. The less defined pathway takes trajectories eastward across the North Atlantic Ocean and over Europe. From there they disperse and enter the Arctic in a disorganized pattern.

Entry regions to the Arctic (70° N) are shown in Fig. 9c. The most prominent entrance region is between Nunavut, Canada and Greenland, a common pathway seen in Fig. 9b. Of the trajectories that enter the Arctic from North America within 15 days, 85% arrive between 40–100° W. A much smaller percentage (14%) enters the Arctic across Northern Europe between 40° W and 40° E. This region also is depicted in Fig. 9b. The remaining 1% enters the Arctic sporadically along the 70° N latitude ring.

The distribution of altitudes at which trajectories arrive in the Arctic (Fig. 9d) is similar to that for the Asian domain (Fig. 4d). Most trajectories arriving from North America enter the Arctic in the middle (42%) and upper troposphere (53%); only 5% arrive in

ACPD
11, 5435–5491, 2011

the lower troposphere. These pathways are consistent with previous studies (Klonecki et al., 2003; Stohl, 2006; Law and Stohl, 2007).

6 North American case study

DC-8 flight 5 on 5 April 2008 contains an example of transport from North America to the Arctic. Leg 8, between 16:27–17:13 UTC, is shown in Fig. 3a as the red segment between Baffin Island, Canada and Disko Bay, Greenland.

6.1 Chemical fingerprinting

Volatile organic compounds, including nonmethane hydrocarbons (NMHCs), generally reach maximum concentrations over the United States during the winter months when OH production and photochemistry are at a seasonal minimum (Russo et al., 2010). Concentrations decline during spring, reaching a minimum during the summer months when photochemistry is most active. Some of these VOCs undergo chemical reactions in the presence of nitrogen oxides to produce ozone, a component of photochemical smog (Carter, 1994; Russo et al., 2010). It is important to note that NMHCs from urban locations in the United States are primarily anthropogenic (Lee et al., 2006).

Figure 10 contains plots of five species with respect to altitude during the 5 April 2008 flight. Similar to the previous figure of this type (Fig. 5), data for flight legs other than leg 8 are in black. However, since all data points in the North American leg represent the sampled plume, the entire suite of data for leg 8 is colored blue. These data were determined to be from the same plume since they all experienced enhancements over their respective background values, and they were sampled in the same altitude range (4500–5000 m).

The incomplete combustion (IC) tracer C_6H_6 (Fig. 10c), as well as two purely anthropogenic tracers (HCFC-22 and C_2Cl_4, Fig. 10d,e), whose origins have been discussed in the previous case study, exhibit enhancements along leg 8. Since our IC tracer

ACPD
11, 5435–5491, 2011

can have either biomass burning or anthropogenic origins, we correlated it with the known anthropogenic species C_2Cl_4 to determine its source. The two are well correlated ($r^2 = 0.72$); thus, we can assume C_6H_6 has anthropogenic sources. In addition, C_2H_6 and C_3H_8 (also enhanced along leg 8, Fig. 10a,b, respectively) – two natural gas tracers that also are emitted from biomass burning – show good correlation with the anthropogenic tracer C_2Cl_4 ($r^2 = 0.86$ and $r^2 = 0.90$, respectively). Therefore, the data suggest that an urban/industrial influence is much more likely than a biomass burning influence.

Similar to Table 2, Table 3 presents mean background mixing ratios of the species discussed above during ARCTAS-A for comparison with mean mixing ratios from the plume sampled along leg 8. The species listed in Table 3 exhibit higher mixing ratios in the leg 8 North American plume than in the background air. Mean values of C_3H_8, C_6H_6, C_2Cl_4, C_2H_6 and HCFC-22 in the North American plume are enhanced by 83, 76, 51, 37 and 3%, respectively, over their mean background values (Table 3).

In summary, two purely anthropogenic species (C_2Cl_4 and HCFC-22) were enhanced over the background in the North American plume. Tetrachloroethene correlated well with benzene, a non-specific tracer of incomplete combustion, as well as two natural gas tracers (C_3H_8 and C_2H_6), strongly suggesting anthropogenic rather than biomass sources. These data suggest that the DC-8 sampled anthropogenic emissions along leg 8 of the ARCTAS flight on 5 April 2008. The North American source is examined further in the next section.

6.2 Transport and meteorology

Backward trajectories were released each minute along flight leg 8 within the 600–500 hPa layer, a total of 47 releases. As before, each trajectory was examined to determine whether it entered the boundary layer along its path; 39 trajectories were found to have done so (Fig. 11a). Boundary layer occurrences of the trajectories in Fig. 11a are shown in Fig. 11b. Most of the trajectories follow a complex looping path as described below. Although a few travel westward across the United States and

ACPD
11, 5435–5491, 2011

encounter the clean boundary layer of the Northern Pacific Ocean, the majority of boundary layer occurrences are located along the east coast of North America where anthropogenic emissions are enhanced (Fig. 2d).

Similar to the previous case, the trajectories in Fig. 11a,b, combined with WRF constant pressure analyses (Fig. 12), are examined to determine the factors contributing to the transport of emissions. Fifteen days prior to the DC-8 sampling anthropogenic emissions, the average location of the East Coast trajectories is over Baffin Bay (Fig. 11a), close to their later sampling location. They then move in a generally looping pattern over Northeastern Canada and the Northeastern US for ~ 10 days (Fig. 11a) due to a series of cyclones and anticyclones in the area. The trajectories are located along the Northeastern US coastline five days prior to the flight (Fig. 12a). It is between 4 and 5 days back from the flight that the most trajectories encounter the boundary layer along the North American coastline where anthropogenic emissions are at their greatest (Figs. 11b, 12a, 2d). A surface low over the Great Lakes places the trajectories in a region of southwesterly flow, transporting them northeastward toward Prince Edward Island. The low strengthens and transports the trajectories into its warm sector 3 days prior to the flight (Fig. 12b). It is here that the trajectories undergo ascent that lofts them into the upper troposphere. Finally, they round the base of a middle tropospheric trough before travelling northwestward to the DC-8.

Figure 11c shows deep ascent beginning ~ 4 days prior to sampling. This corresponds to the time that the trajectories are located within the cyclone's warm sector (Fig. 12b). Thus, a WCB was suspected to be the cause of the ascent. The methods used previously to define "reasonably strong" WCB transport (Eckhardt et al., 2004) again were employed. All of the trajectories examined along leg 8 satisfy the horizontal WCB requirements. The tropopause height was calculated between 40° N and 60° N, yielding an average height of 9644 m, with 60% of this value being 5787 m. Although 44% of the trajectories meet the 15–22 K increase in potential temperature criterion, none satisfy the ascent criterion. However, if we reduce the vertical criterion to 40% of the tropopause height (3858 m), 72% of the trajectories satisfy the requirement.

ACPD
11, 5435–5491, 2011

Furthermore, 94% of those satisfying the potential temperature criterion also satisfy the revised ascent criterion. Considering horizontal motion, the change in potential temperature, and the reduced ascent criterion, 74% of the examined leg 8 trajectories satisfy the revised WCB requirement. It is important to note the strong seasonal variability in WCB frequency and associated vertical mass flux, with maxima during winter and minima in summer (Stohl, 2001; Eckhardt et al., 2004). Since ARCTAS-A occurred during a transitional season, the 60% ascent requirement may be too strict for spring, causing valid WCBs to be neglected. This information and the synoptic patterns described above indicate that the leg 8 trajectories most likely experienced ascent due to a WCB.

To summarize, chemical fingerprinting and meteorological analyses indicate that the DC-8 sampled North American anthropogenic emissions during leg 8 of the 5 April 2008 flight. Vertical distribution plots and comparisons with background mixing ratios revealed enhancements during this leg, including tracers having purely anthropogenic sources. Trajectory analysis showed that boundary layer air was encountered along the Northeastern US coast where anthropogenic emissions are a maximum (Fig. 2d). Finally, the trajectories underwent suspected WCB related ascent to the middle troposphere where the emissions were sampled by the DC-8.

7 European transport during ARCTAS-A

Fifteen day forward trajectories were launched from the 224 grid points with European anthropogenic emissions (Fig. 2e,f) on each of the 31 ARCTAS-A days, producing a total of 6944 releases. Only a few release points in the far southeastern domain do not produce Arctic bound trajectories within the 15 day period (Fig. 13a). Of the total trajectories released, 1936 (28%) reach the Arctic within 15 days. Trajectories released at latitudes greater than 50° N account for 32% of the trajectories entering the Arctic (70° N). Fifty-four percent of the trajectories released between 40° N and 50° N reach the Arctic, while latitudes less than 40° N account for the remaining 14%. Trajecto-

ACPD
11, 5435–5491, 2011

ries reaching the Arctic follow two distinct pathways (Fig. 13b). The first transports emissions northward across Northern Europe before crossing 70° N. This path is most common for trajectories that remain in the lower troposphere. The second common pathway begins with the trajectories moving eastward from the domain. They cross Turkey and continue eastward across the Northern Middle East and then to the Arctic. Although this pathway is most common for trajectories in the middle and upper troposphere, some trajectories in the middle and upper levels follow the first pathway.

Locations over Northern Europe and Northeastern Russia are the dominant entry region to the Arctic for trajectories originating from the European domain (Fig. 13c). This 70° longitude region between 20–90° E accounts for 62% of the trajectories entering the Arctic. This sector differs considerably from those observed for Asian and North American trajectories (Figs. 4c and 9c, respectively). The longitude sector between 180° W and 140° W was a frequent entry region for Asian emissions (61.5%), but it accounts for only 6% of the trajectories entering the Arctic from Europe. Likewise, the region between 100° W and 40° W was a common entry region for North American trajectories (85%), but it accounts for only 7% of the trajectories released from the European domain. Thus, considering the combination of all three anthropogenic source regions, the releases enter the Arctic over a wide range of longitudes.

The altitudes at which European trajectories enter the Arctic (Fig. 13d) differ from the previous two domains (Figs. 4d and 9d). European releases arrive in the lower, middle, and upper troposphere, whereas trajectories from the previous domains were primarily in the middle and upper troposphere. Although the middle troposphere accounts for 56% of the European releases reaching the Arctic, the lower levels account for 17%. This percentage arriving in the lower troposphere is considerably greater than the previous two regions (3% from Asia and 5% from North America). This finding of European arrivals in the lower troposphere is consistent with findings by Klonecki et al. (2003), Stohl (2006), and Law and Stohl (2007). The remaining 27% of Arctic bound trajectories from Europe arrive in the upper levels.

ACPD
11, 5435–5491, 2011

8 European case study

Data from DC-8 flight 8 on 12 April 2008 comprise our case study of European emissions. This is the same flight on which Asian emissions were sampled, emphasizing the finding that many ARCTAS-A flights sampled air with multiple origins. The case focuses on the period 18:26–18:55 UTC which is denoted as leg 8 (leg 5 was studied for the Asian case). Leg 8 is located across the Bering Strait and over St. Lawrence Island, AK (Fig. 3b).

8.1 Chemical fingerprinting

We are not aware of previous research that provides a chemical fingerprint that is specific to European anthropogenic emissions. Thus, chemical considerations will not definitively link the sampled plume to a European source. Rather, the firm linkage with Europe will be based on trajectory and meteorological analyses.

The species examined for this case study are C_2Cl_4, C_2H_2, C_6H_6, C_2H_6, C_3H_8 and methane (CH_4) (Fig. 14). Similar to the other cases, the blue points (in Fig. 14) represent the sampled plume along leg 8. This plume consists of 3 data points at almost the same altitude between 3704–3708 m. Each of the tracers being examined has been used and discussed in previous sections with the exception of CH_4. Methane is introduced because when CH_4, C_2H_6 and C_3H_8 are well correlated, natural gas emission can be inferred (Sect. 2.3). However, since CH_4, C_3H_8 and C_2H_6 emissions can be from both biomass and anthropogenic sources, further examination is needed. First, the correlation for each of the natural gas tracers with the others was computed. The best correlations are between C_2H_6 and C_3H_8 ($r^2 = 0.95$), followed by CH_4 and C_3H_8 ($r^2 = 0.76$), and CH_4 and C_2H_6 ($r^2 = 0.56$). In addition to the fair to strong mutual correlations, this trio of gases also exhibits excellent correlation with the urban/industrial tracer C_2Cl_4 ($r^2 = 0.91$, 0.83 and 0.96 for CH_4, C_2H_6 and C_3H_8, respectively). This strongly suggests that CH_4, C_2H_6 and C_3H_8 were co-emitted from an urban/industrial source such as natural gas usage, and not from biomass burning. Because ethane

ACPD
11, 5435–5491, 2011

is the second most abundant component of natural gas after CH_4 (Xiao et al., 2008), the relatively weaker correlations of CH_4 with C_2H_6 and C_3H_8 may suggest that an additional urban source of CH_4 also was present, or that the strong C_2H_6 and C_3H_8 correlations represent a different fossil fuel source such as liquefied petroleum gas (LPG). Regardless, the light alkane signal is found to be urban in origin. Indeed, the two IC tracers (C_2H_2 and C_6H_6) also show excellent correlation with C_2Cl_4 ($r^2 = 0.99$ and 0.73, respectively), again consistent with an urban/industrial combustion source and not biomass burning.

Following the previously described methodology, Table 4 presents mean background mixing ratios during ARCTAS-A for the tracers used in this case, as well as mean values for the sampled plume along leg 8. Similar to the previous two cases (Tables 2–3), the species in Table 4 have higher mixing ratios in the leg 8 European plume than in the background air measured during ARCTAS-A. Mean values of C_6H_6, C_2H_2, C_3H_8, C_2Cl_4, C_2H_6 and CH_4 in the European plume are enhanced by 129, 97, 72, 44, 36 and 2%, respectively, over their mean background values (Table 4).

In summary, enhancements in the purely anthropogenic tracer C_2Cl_4 indicate that our plume is of anthropogenic origin. Generally good correlations between CH_4, C_2H_6, C_3H_8, C_2Cl_4, C_6H_6 and C_2H_2 also show that anthropogenic emissions including combustion sources and possibly natural gas sources were sampled along leg 8 of DC-8 flight 8 on 12 April 2008. The source of these emissions will be examined in the next section.

8.2 Transport and meteorology

Of all the DC-8 flights during April, flight 8 provides the most favorable trajectories for sampling boundary layer air over Europe, while avoiding large areas of biomass burning. A backward trajectory was released each minute along leg 8 within the 850–500 hPa layer. Of the 30 total trajectories, 13 travel in the boundary layer at some time during their 15 day transit (Fig. 15a). The remaining 17 trajectories released along leg 8 follow pathways that are similar to the boundary layer trajectories, but always remain

ACPD
11, 5435–5491, 2011

above the boundary layer.

Knowing where the trajectories were in the boundary layer is especially important in this case because of a large area of fires across Western Russia. Figure 16 shows a close up view of the trajectories from Fig. 15a, as well as a composite of all fire locations between 26 March and 6 April 2008 (the period when the trajectories were over Europe and Russia). Fire locations are from the Naval Research Laboratory (NRL) Fire Locating and Modeling of Biomass Burning Emissions (FLAMBE) dataset (Reid et al., 2009). The fires primarily are located between 50–60° N, with their westernmost boundary across Eastern Belarus and Northeastern Ukraine. Figure 15b shows the boundary layer segments of the trajectories in Fig. 15a. A few trajectories have brief encounters with the boundary layer over Western Russia, near the large region of fires. However, these brief incursions are not evident in the chemical data just described. Instead, most trajectories encounter the boundary layer across Europe, where fires are virtually absent.

One simple pathway encompasses most of the trajectories in Fig. 15a. Fifteen days prior to aircraft sampling (Fig. 15a), the average location of the leg 8 trajectories is near 30° W over the Northern Atlantic Ocean in a region of westerly flow. They continue in this westerly flow for several days and then pass over Western Europe where they encounter the boundary layer (Fig. 17a) in an area of enhanced anthropogenic emissions (Fig. 2f). When the trajectories are near Poland, 11 days prior to sampling (not shown), the flow becomes stagnant. Over the next two days, they drift eastward as a surface low develops over the Atlantic and moves onshore near Norway. The trajectories pass into the cyclone's warm sector where they begin to ascend 7 days prior to sampling (Fig. 17b). Once lofted into the upper troposphere, they are transported by the westerlies and are sampled by the DC-8.

Figure 15c presents the trajectories from Fig. 15a in a pressure versus time reference. Synoptic scale ascent is indicated between ~ 6–8 days prior to sampling. Similar to the previous cases, this is when the trajectories are in a cyclone's warm sector (Fig. 17b). Thus, potential WCB influences again were investigated using the criteria

ACPD
11, 5435–5491, 2011

in Eckhardt et al. (2004). Ninety-two percent of the 13 trajectories examined satisfy the horizontal WCB criteria. The average tropopause height in the latitude belt 60–70° N was 9584 m, with 60% of this value being 5751 m. Only 1 of the 13 trajectories satisfies the 48 h ascent requirement. Similar to the previous case, if the ascent criterion is decreased to 40% of the tropopause height (3834 m) during a 48 h period, 62% of the 13 trajectories meet the revised requirement. It is important to note that Figs. 15a and 16 show two separate groups of trajectories. The smaller group passes over Greenland and is not suspected to have undergone WCB processes. If we remove these 3 "stray" trajectories, 80% of the remainder satisfies the revised WCB requirements. Therefore, we believe it is probable that the trajectories' large scale ascent is due to a WCB.

In summary, these results strongly suggest that the DC-8 sampled anthropogenic emissions along leg 8 of the 12 April 2008 flight. Vertical distributions showed enhancements in the purely anthropogenic tracer C_2Cl_4, as well as in natural gas tracers CH_4, C_2H_6 and C_3H_8, determined to be of anthropogenic origins. The IC tracers C_2H_2 and C_6H_6 were shown to be of anthropogenic origin as well. Trajectory analysis showed that boundary layer encounters occurred across European locations with enhanced anthropogenic emissions (Fig. 2f). The leg 8 trajectories were lofted into the upper troposphere, most likely by a WCB, where they were subsequently sampled by the DC-8. Although the pathway taken by these trajectories was common during ARCTAS-A (Sect. 3.6), they did not enter the Arctic in the most common region (Northern Europe/Northeastern Russia, Fig. 13c). Instead, the trajectories entered the Arctic through one of the secondary "hot spots" (Fig. 13c). This secondary location, north of the Bering Strait is shared by emissions from Asia (Fig. 4c).

9 Summary and conclusions

This study has examined the transport of anthropogenic emissions to the Arctic during NASA's ARCTAS field mission conducted during 2008 (Jacob et al., 2010). Our focus was the spring phase of ARCTAS (ARCTAS-A) that occurred during April. Although

ACPD
11, 5435–5491, 2011

biomass burning emissions dominated pollution transport to the Arctic during the study period (Warneke et al., 2009; Jacob et al., 2010), our goal was to document the Arctic transport and meteorology associated with anthropogenic emissions. Three source regions were studied, namely Asia, North America, and Europe. Meteorological data were obtained from high resolution simulations using the Weather Research and Forecasting (WRF) model. We computed statistics describing common pathways, origins, and entry regions for emissions entering the Arctic (defined as 70° N) during the complete ARCTAS-A period. We also presented a detailed case study for each source region using DC-8 aircraft-derived in situ data and backward trajectories.

Leg 5 from DC-8 flight 8 on 12 April 2008 was found to have sampled anthropogenic emissions originating from Eastern Asia. Results showed enhancements of several key tracers (OCS, CH_3Cl, 1,2-DCE, and H-1211) that Barletta et al. (2009) have linked to Eastern Asian anthropogenic emissions. Values of the purely anthropogenic species HCFC-22 and C_2Cl_4 also were enhanced along this leg. Carbonyl sulphide and CH_3Cl, two tracers that could have either biomass burning or anthropogenic origins, were highly correlated with the anthropogenic tracer C_2Cl_4, which led to the conclusion that both tracers had anthropogenic origins.

Fifteen day backward trajectories released from leg 5 were traced back to origins across Eastern Asia. They originated along the Eastern Asian coast and passed through the boundary layer in regions of anthropogenic emissions. The pathway, origin, and Arctic entry locations of this case study were consistent with those of the entire ARCTAS-A period. Meteorological analyses highlighted the importance of synoptic scale cyclones and anticyclones in transporting the emissions. The results also illustrated the importance of a warm conveyor belt (WCB) in transporting the emissions to higher altitudes where they were sampled by the DC-8. Based on its chemical signature and backward trajectories, leg 5 of flight 8 was concluded to exhibit an anthropogenic influence.

The transport of Asian anthropogenic emissions also was investigated each day during ARCTAS-A, producing a “climatology” of the period. Based on 15 day

ACPD
11, 5435–5491, 2011

forward trajectories, Asian emissions during ARCTAS-A most commonly were transported eastward across the Northern Pacific Ocean and then lofted into the upper levels. The coast of Eastern Asia is a common location for the development of strong WCBs (Eckhardt et al., 2004), and we hypothesize that Asian transport to the Arctic often is facilitated by them. These emissions usually passed northward through the Bering Sea where they crossed 70° N latitude and entered the Arctic. Results showed that emissions from Asia most commonly entered the Arctic in the middle and upper levels during ARCTAS-A. Emissions that originated from higher latitudes across Eastern Asia tended to arrive in the middle troposphere, while emissions originating at lower latitudes more commonly arrived in the upper troposphere.

Results showed that anthropogenic emissions from North America were sampled along leg 8 of DC-8 flight 5 on 5 April 2008. This period served as our case study. Enhanced mixing ratios of several species, including two having strictly anthropogenic origins (C_2Cl_4 and HCFC-22), were found along the leg. The incomplete combustion tracer C_6H_6 exhibited a good correlation with the purely anthropogenic tracer C_2Cl_4 and was determined to have anthropogenic origins. Similarly, two natural gas tracers (C_2H_6 and C_3H_8) also correlated well with C_2Cl_4 indicating their origins were from anthropogenic sources.

Backward trajectories released along leg 8 spent considerable time over North America. They were within the boundary layer over regions of known anthropogenic emissions, especially the US Northeast Corridor. Since WCBs frequently originate east of North America (Eckhardt et al., 2004), it was not surprising that a WCB likely was responsible for the vertical transport of these emissions to their sampling locations at the DC-8.

The transport pathway of the North American case was consistent with transport statistics for the entire ARCTAS-A period. Emissions from North America generally traveled northeast across the far Northwestern Atlantic and over the Labrador Sea. The emissions typically were lofted into the middle and upper troposphere along this path, with the ascent suspected to be commonly due to WCBs. Once lofted, the trajectories

ACPD
11, 5435–5491, 2011

generally entered the Arctic in a region extending between Western Nunavut, Canada and Central Greenland. Similar to results for Asian anthropogenic emissions, trajectories that originated in the higher latitudes of North America typically entered the Arctic in the middle troposphere, while emissions from lower latitudes more frequently arrived in the upper troposphere.

Anthropogenic emissions from Europe were sampled along leg 8 of flight 8 on 12 April 2008. This conclusion is based on several factors. The purely anthropogenic tracer C_2Cl_4 was enhanced along this leg. Generally good correlations between CH_4, C_2H_6 and C_3H_8 suggested an influence from an evaporative urban fossil fuel source such as natural gas and/or liquefied petroleum gas. These light alkanes were also well correlated with the purely anthropogenic tracer C_2Cl_4. Similarly, enhanced mixing ratios of C_2H_2 and C_6H_6 also were found along leg 8, and since they were well correlated with C_2Cl_4, they were determined to have been from anthropogenic combustion sources as opposed to biomass burning.

Backward trajectories released along leg 8 indicated that the sampled air had passed within the boundary layer over Eastern and Western Europe. These are areas shown to have enhancements in anthropogenic emissions (Fig. 2f). Although WCBs seldom begin over Europe, a WCB was thought to be responsible for the trajectories' ascent from the lower to the upper troposphere where they were sampled by the DC-8.

Our ARCTAS-A transport "climatology" revealed that European anthropogenic emissions frequently traveled northward out of Europe, entering the Arctic across Northern Europe and Northeastern Russia. Although this scenario was the most common method by which trajectories reached the Arctic, some emissions, including those from our case study, traveled eastward between 50–70° N to a wide range of Arctic entry locations along 70° N. Unlike the Asian and North American domains, emissions that originated in the higher latitudes of Europe more frequently entered the Arctic in the lower troposphere, while emissions originating further south arrived in the middle and upper troposphere.

ACPD
11, 5435–5491, 2011

Although biomass burning emissions dominated Arctic transport during ARCTAS-A (e.g., Warneke et al., 2009; Jacob et al., 2010), the current results emphasize that the historically important anthropogenic emissions cannot be neglected. In the future, biomass burning typically may be the dominant source of Arctic pollution due to increasing global temperatures that will promote enhanced numbers of wildfires.

Acknowledgement. The research at Florida State University was sponsored by the NASA Tropospheric Chemistry Program under Grant NNX0AH72G. The research at the University of California-Irvine was supported by NASA grant NNX09AB22G. We would like to express our sincere thanks to everyone who participated in the highly successful ARCTAS mission.

References

Anderson, B. E., Grant, W., Gregory, G., Browell, E., Collins Jr., J., Sachse, G., Bagwell, D., Hudgins, C., Blake, D., and Blake, N.: Aerosols from biomass burning over the south tropical Atlantic region: distributions and impacts, J. Geophys. Res., 101(D19), 24117–24138, 1996.

Aucott, M. L., McCulloch, A., Graedel, T. E., Kleiman, G., Midgley, P., and Li, Y.-F.: Anthropogenic emissions of trichloromethane (chloroform, $CHCl_3$) and chlorodifluoromethane (HCFC-22): reactive chlorine emissions inventory, J. Geophys. Res., 104, 8405–8415, 1999.

Barletta, B., Meinardi, S., Simpson, I. J., Atlas, E. L., Beyersdorf, A. J., Baker, A. K., Blake, N. J., Yang, M., Midyett, J. R., Novak, B. J., McKeachie, R. J., Fuelberg, H. E., Sachse, G. W., Avery, M. A., Campos, T., Weinheimer, A. J., Rowland, F. S., and Blake, D. R.: Characterization of volatile organic compounds (VOCs) in Asian and north American pollution plumes during INTEX-B: identification of specific Chinese air mass tracers, Atmos. Chem. Phys., 9, 5371–5388, doi:10.5194/acp-9-5371-2009, 2009.

Barrie, L. A. and Hoff, R. M.: Five years of air chemistry observations in the Canadian Arctic, Atmos. Environ., 19, 1995–2010, 1985.

Barrie, L. A., Bottenheim, J. W., and Hart, W. R.: Polar sunrise experiment 1992 (PSE 1992): preface, J. Geophys. Res., 99, 25313–25314, 1994.

Blake, N. J., Blake, D. R., Sive, B. C., Chen, T.-Y., Rowland, F. S., Collins Jr., J. E., Sachse, G. W., and Anderson, B. E.: Biomass burning emissions and vertical distribution

ACPD

11, 5435–5491, 2011

of atmospheric methyl halide and other reduced carbon gases in the South Atlantic region, J. Geophys. Res., 101(D19), 24151–24164, 1996.

Blake, N. J., Blake, D. R., Simpson, I. J., Meinardi, S., Swanson, A. L., Lopez, J. P., Katzenstein, A. S., Barletta, B., Shirai, T., Atlas, E., Sachse, G., Avery, M., Vay, S., Fuelberg, H. E., Kiley, C. M., Kita, K., and Rowland, F. S.: NMHCs and halocarbons in Asian continental outflow during the transport and chemical evolution over the Pacific (TRACE-P) field campaign: comparison with PEM-West B, J. Geophys. Res., 108(D20), 8806, doi:10.1029/2002JD003367, 2003.

Blake, N. J., Streets, D. G., Woo, J., Simpson, I. J., Green, J., Meinardi, S., Kita, K., Atlas, E., Fuelberg, H. E., Sachse, G., Avery, M. A., Vay, S. A., Talbot, R. W., Dibb, J. E., Bandy, A. R., Thornton, D. C., Rowland, F. S., and Blake, D. R.: Carbonyl sulfide and carbon disulfide: large-scale distributions over the Western Pacific and emissions from Asia during TRACE-P, J. Geophys. Res., 109, D15S05, doi:10.1029/2003JD004259, 2004.

Blake, D.: Whole air sampling (WAS) from the DC-8 aircraft during ARCTAS, 2008, available at: http://www.espo.nasa.gov/arctas/docs/instruments/was.pdf, 2008.

Bradley, R. S., Keiming, F. T., and Diaz, H. F.: Climatology of surface-based inversions in the North American Arctic, J. Geophys. Res., 97, 15699–15712, 1992.

Butler, J. H., Montzka, S. A., Clarke, A. D., Lobert, J. M., and Elkins, J. W.: Growth and distribution of halons in the atmosphere, J. Geophys. Res., 103(D1), 1503–1511, 1998.

Carlson, T. N.: Speculations on the movement of polluted air to the Arctic, Atmos. Environ., 15, 1473–1477, 1981.

Carter, W. P. L.: Development of ozone reactivities for volatile organic compounds, JAPCA J. Air Waste Ma., 44, 881–899, 1994.

Curry, J. A.: On the formation of continental polar air, J. Atmos. Sci., 40, 2279–2292, 1983.

Curry, J. A.: The contribution of radiative cooling to the formation of cold-core anticyclone, J. Atmos. Sci., 44, 2575–2592, 1987.

Ding, A., Wang, T., Xue, L., Gao, J., Stohl, A., Lei, H., Jin, D., Ren, Y., Wang, X., Wei, X., Qi, Y., Liu, J., and Zhang, X.: Transport of North China air pollution by midlatitude cyclones: case study of aircraft measurements in summer 2007, J. Geophys. Res., 114, D08304, doi:10.1029/2008JD011023, 2009.

Eckhardt, S., Stohl, A., Beirle, S., Spichtinger, N., James, P., Forster, C., Junker, C., Wagner, T., Platt, U., and Jennings, S. G.: The North Atlantic Oscillation controls air pollution transport to the Arctic, Atmos. Chem. Phys., 3, 1769–1778, doi:10.5194/acp-3-1769-2003, 2003.

ACPD
11, 5435–5491, 2011

Eckhardt, S., Stohl, A., Wernli, H., James, P., Forster, C., and Spichtinger, N.: A 15-year climatology of warm conveyor belts, J. Climate, 17, 218–237, 2004.
Fraser, P. J., Oram, D. E., Reeves, C. E., Penkett, S. A., and McCulloch, A.: Southern hemispheric halon trends (1978–1998) and global halon emissions, J. Geophys. Res., 104(D13), 15985–16000, 1999.
Fuelberg, H. E., Loring Jr., R. O., Watson, M. V., Sinha, M. C., Pickering, K. E., Thompson, A. M., Sachse, G. W., Blake, D. R., and Schoeberl, M. R.: TRACE-A trajectory intercomparison. 2. Isentropic and kinematic methods, J. Geophys. Res., 101, 23927–23939, 1996.
Fuelberg, H. E., Hannan, J. R., van Velthoven, P. F. J., Browell, E. V., Bieberbach Jr., G., Knabb, R. D., Gregory, G. L., Pickering, K. E., and Selkirk, H. B.: A meteorological overview of the SONEX period, J. Geophys. Res., 105, 3633–3651, 2000.
Fuelberg, H. E., Harrigan, D. L., and Sessions, W.: A meteorological overview of the ARCTAS 2008 mission, Atmos. Chem. Phys., 10, 817–842, doi:10.5194/acp-10-817-2010, 2010.
Hileman, B.: Arctic haze, Environ. Sci. Technol., 17(6), 232–236, doi:10.1021/es00112a602, 1983.
Hoff, R. M.: Vertical structure of Arctic haze observed by lidar, J. Appl. Meteorol., 27, 125–139, 1987.
Iverson, T.: On the atmospheric transport of pollution to the Arctic, Geophys. Res. Lett., 11, 457–460, 1984.
Jacob, D. J., Crawford, J. H., Maring, H., Clarke, A. D., Dibb, J. E., Emmons, L. K., Ferrare, R. A., Hostetler, C. A., Russell, P. B., Singh, H. B., Thompson, A. M., Shaw, G. E., McCauley, E., Pederson, J. R., and Fisher, J. A.: The Arctic Research of the Composition of the Troposphere from Aircraft and Satellites (ARCTAS) mission: design, execution, and first results, Atmos. Chem. Phys., 10, 5191–5212, doi:10.5194/acp-10-5191-2010, 2010.
Kasischke, E. S., Hyer, E. J., Novelli, P. C., Bruhwiler, L. P., French, N. H. F., Sukhinin, A. I., Hewson, J. H., and Stocks, B. J.: Influences of boreal fire emissions on Northern Hemisphere atmospheric carbon and carbon monoxide, Global Biogeochem. Cy., 19, GB1012, doi:10.1029/2004GB002300, 2005.
Katzenstein, A. S., Doezema, L. A., Simpson, I. J., Blake, D. R., and Rowland, F. S.: Extensive regional atmospheric hydrocarbon pollution in the Southwestern United States, P. Natl. Acad. Sci. USA, 100, 11975–11979, 2003.
Kettle, A. J., Kuhn, U., von Hobe, M., Kesselmeier, J., and Andreae, M. O.: Global budget of

ACPD
11, 5435–5491, 2011

carbonyl sulfide: temporal and spatial variations of the dominant sources and sinks, J. Geophys. Res., 107(D22), 4658, doi:10.1029/2002JD002187, 2002.
Klonecki, A., Hess, P., Emmons, L., Smith, L., and Orlando, J.: Seasonal changes in the transport of pollutants into the Arctic troposphere-model study, J. Geophys. Res., D4, 8367, doi:1029/2002JD002199, 2003.
Kondo, Y., Sahu, L., Moteki, N., Takegawa, N., Matsui, H., Zhao, Y., Vay, S., Diskin, G. S., Anderson, B., Wisthaler, A., Jimenez, J. L., Fuelberg, H. E., Huey, G., Weinheimer, A. J., and Brune, W. H.: Emissions of black carbon and organic aerosols from forest fires in Canada and Russia in 2008, in press, J. Geophys. Res., 2011.
Law, K. S. and Stohl, A.: Arctic air pollution: origins and impacts, Science, 315, 1537–1540, doi:10.1126/science.1137695, 2007.
Lee, B. H., Munger, J. W., Wofsy, S. C., and Goldstein, A. H.: Anthropogenic emissions of nonmethane hydrocarbons in the Northeastern United States: measured seasonal variations from 1992–1996 and 1999–2001, J. Geophys. Res., 111, D20307, doi:10.1029/2005JD006172, 2006.
Li, S. M. and Barrie, L. A.: Biogenic sulphur aerosols in the Arctic troposphere. 1. Contributions to sulphate, J. Geophys. Res., 98D, 20613–20622, 1993.
Martin, B. D., Fuelberg, H. E., Blake, N. J., Crawford, J. H., Logan, J. A., Blake, D. R., and Sachse, G. W.: Long range transport of Asian outflow to the Equatorial Pacific, J. Geophys. Res., 108(D2), 8322, doi:10.1029/2001JD001418, 2002.
Matsui, H., Kondo, Y., Moteki, N., Takegawa, N., Sahu, L. K., Zhao, Y., Fuelberg, H. E., Sessions, W., Diskin, G., Blake, D. R., and Wisthaler, A.: Seasonal variation of the transport of black carbon aerosol from the Asian continent to the Arctic during the ARCTAS aircraft campaign, J. Geophys. Res., in press, 2011.
Meyer, F. G., Curry, J. A., Brock, C. A., and Radke, L. F.: Springtime visibility in the Arctic, J. Appl. Meteorol., 30, 342–357, 1990.
Mitchell Jr., J. M.: Visual range in the polar regions with particular reference to the Alaskan Arctic, J. Clim. Appl. Meteorol., 23, 916–928, 1957.
Montzka, S. A., Hall, B. D., and Elkins, J. A.: Accelerated increases observed for hydrochlorofluorocarbons since 2004 in the global atmosphere, Geophys. Res. Lett., 36, L03804, doi:10.1029/2008GL036475, 2009.
Oltmans, S. J., Lefohn, A. S., Harris, J. M., Tarasick, D. W., Thompson, A. M., Wernli, H., Johnson, B. J., Davies, J., Novelli, P. C., Montzka, S. A., Sweeney, C., Patrick, L. A., Jefferson, A.,

ACPD
11, 5435–5491, 2011

Dann, T., Ray, J. D., and Shapiro, M.: Enhanced ozone over Western North America from biomass burning in Eurasia during April 2008 as seen in surface and profile observations, submitted, Atmos. Environ., 44, 4497–4509, 2010.
Quinn, P. K., Miller, T. L., Bates, T. S., Ogren, J. A., Andrews, E., and Shaw, G. E.: A three-year record of simultaneously measured aerosol chemical and optical properties at Barrow, Alaska, J. Geophys. Res., 107(D11), doi:10.1029/2001JD001248, 2002.
Raatz, W. E. and Shaw, G. E.: Long-range tropospheric transport of pollution aerosols in the Alaskan Arctic, J. Clim. Appl. Meteorol., 23, 1052–1064, 1984.
Raatz, W. E.: The climatology and meteorology of Arctic air pollution, in: Pollution of the Arctic Atmosphere, edited by: Sturges, W. T., Elsevier, New York, 13–42, 1991.
Reid, J., Hyer, E. J., Prins, E. M., Westphal, D. L., Zhang, J., Wang, J., Christopher, S. A., Curtis, C. A., Schmidt, C. A., Eleuterio, D. P., Richardson, K. A., and Hoffman, J. P.: Global Monitoring and Forecasting of Biomass Burning Smoke: Description of and Lessons From the Fire Locating and Modeling of Burning Emissions (FLAMBE) Program, IEEE J. Sel. Top. Appl., 2, 144–162, 2009.
Rinke, A., Dethloff, K., and Fortmann, M.: Regional climate effects of Arctic haze, Geophys. Res. Lett., 31, L16202, 2004.
Russo, R., Talbot, R. W., Dibb, J. E., Scheuer, E., Seid, G., Jordan, C. E., Fuelberg, H. E., Sachse, G. W., Avery, M. A., Vay, S. A., Blake, D. R., Blake, N. J., Atlas, E., Fried, A., Sandholm, S. T., Tan, D., Singh, H. B., Snow, J., and Heikes, B. G.: Chemical composition of Asian continental outflow over the Western Pacific: results from transport and chemical evolution over the Pacific (TRACE-P), J. Geophys. Res., 108(D20), 8804, doi:10.1029/2002JD003184, 2003.
Russo, R. S., Zhou, Y., White, M. L., Mao, H., Talbot, R., and Sive, B. C.: Multi-year (2004–2008) record of nonmethane hydrocarbons and halocarbons in New England: seasonal variations and regional sources, Atmos. Chem. Phys., 10, 4909–4929, doi:10.5194/acp-10-4909-2010, 2010.
Sachse, G. W., Hill, G. F., Wade, L. O., and Perry, M. G.: Fast-response, high-precision carbon monoxide sensor using a tunable diode laser absorption technique, J. Geophys. Res., 92, 2071–2081, 1987.
Sachse, G. W., Harriss, R. C., Fishman, J., Hill, G. F., and Cahoon, D. R.: Carbon monoxide over the Amazon basin during the 1985 dry season, J. Geophys. Res., 93, 1422–1430, 1988.
Schnell, R. C.: Arctic haze and the Arctic gas aerosol sampling program (AGASP), Geophys.

ACPD
11, 5435–5491, 2011

Res. Lett., 11, 361–364, 1984.
Shaw, G. E.: The Arctic haze phenomenon, B. Am. Meteorol. Soc., 76, 2403–2413, 1995.
Shaw, G. E.: Evidence for a Central Eurasian source area of Arctic haze in Alaska, Nature, 299, 815–818, 1983.
Simpson, I. J., Meinardi, S., Blake, N. J., Rowland, F. S., and Blake, D. R.: Long-term decrease in the global atmospheric burden of tetrachloroethene (C_2Cl_4), Geophys. Res. Lett., 31, L08108, doi:10.1029/2003GL019351, 2004.
Simpson, I. J., Blake, N. J., Barletta, B., Diskin, G. S., Fuelberg, H. E., Gorham, K., Huey, L. G., Meinardi, S., Rowland, F. S., Vay, S. A., Weinheimer, A. J., Yang, M., and Blake, D. R.: Characterization of trace gases measured over Alberta oil sands mining operations: 76 speciated C_2–C_{10} volatile organic compounds (VOCs), CO_2, CH_4, CO, NO, NO_2, NO_y, O_3 and SO_2, Atmos. Chem. Phys., 10, 11931–11954, doi:10.5194/acp-10-11931-2010, 2010.
Singh, H. B., Anderson, B. E., Brune, W. H., Cai, C., Crawford, J. H., Cohen, R. C., Czech, E. P., Emmons, L., Fuelberg, H. E., Huey, G., Jacob, D. J., Jimenez, J. L., Kondo, Y., Kaduwela, A., Mao, J., Olson, J. R., Sachse, G. W., Vay, S. A., Weinheimer, A., Wennberg, P. O., and Wisthaler, A.: Pollution influences on atmospheric composition and chemistry at high northern latitudes: boreal and California forest fire emissions, Atmos. Environ., 44, 4553–4564, 2010.
Skamarock, W. C., Klemp, J. B., Dudhia, J., Gill, D. O., Barker, D. M., Duda, M. G., Huang, X., Wang, W., and Powers, J. G.: A description of the Advanced Research WRF version 3. NCAR Tech. Note NCAR/TN-475+STR, National Center for Atmospheric Research (NCAR), http://www.mmm.ucar.edu/wrf/users/docs/arw_v3.pdf, 113 pp., 2008.
Stohl, A.: A 1-year Lagrangian "climatology" of airstreams in the Northern Hemisphere troposphere and lowermost stratosphere, J. Geophys. Res., 106(D7), 7263–7279, 2001.
Stohl, A.: Characteristics of atmospheric transport into the Arctic troposphere, J. Geophys Res., D11306, doi:1029/2005JD006888, 2006.
Stohl, A. and Law, K.: IGACtivities Newslett., 33, 16–32, 2006, available at: http://www.igac.noaa.gov/newsletter/igac33/May_2006_IGAC_33.pdf.
Stohl, A., Wotawa, G., Seibert, P., and Kromp-Kolb, H.: Interpolation errors in wind fields as a function of spatial and temporal resolution and their impact on different types of kinematic trajectories, J. Appl. Meteorol., 34, 2149–2165, 1995.
Stohl, A., Hittenberger, M., and Wotawa, B.: Validation of the Lagrangian particle dispersion model FLEXPART against large scale tracer experiments, Atmos. Environ., 32, 4245–4264,

ACPD
11, 5435–5491, 2011

1998.
Stohl, A., Eckhardt, S., Forster, C., James, P., and Spichtinger, N.: On the pathways and timescales of intercontinental air pollution transport, J. Geophys. Res. 107(D23), 4684, doi:10.1029/2001JD001396, 2002.
Streets, D. G., Bond, T. C., Carmichael, G. R., Fernandes, S. D., Fu, Q., He, D., Klimont, Z., Nelson, S. M., Tsai, N. Y., Wang, M. Q., Woo, J. H., and Yarber, K. F.: An inventory of gaseous and primary aerosol emissions in Asia in the year 2000, J. Geophys. Res., 108(D21), 8809, doi:10.1029/2002JD003093, 2003.
Warneke, C., McKeen, S. A., de Gouw, J. A., Goldan, P. D., Kuster, W. C., Holloway, J. S., Williams, E. J., Lerner, B. M., Parrish, D. D., Trainer, M., Fehsenfeld, F. C., Kato, S., Atlas, E. L., Baker, A., and Blake, D. R.: Determination of urban volatile organic compound emission ratios and comparison with an emissions database, J. Geophys. Res., 112, D10S47, doi:10.1029/2006JD007930, 2007.
Warneke, C., Bahreini, R., Brioude, J., Brock, C. A., de Gouw, J. A., Fahey, D. W., Froyd, K. D., Holloway, J. S., Middlebrook, A., Miller, L., Montzka, S., Murphy, D. M., Peischl, J., Ryerson, T. B., Schwarz, J. P., Spackman, J. R., and Veres, P.: Biomass burning in Siberia and Kazakhstan as an important source for haze over the Alaskan Arctic in April 2008, Geophys. Res. Lett., 36, L02813, doi:10.1029/2008GL036194, 2009.
Warneke, C., Froyd, K. D., Brioude, J., Bahreini, R., Brock, C. A., Cozic, J., de Gouw, J. A., Fahey, D. W., Ferrare, R., Holloway, J. S., Middlebrook, A. M., Miller, L., Montzka, S., Schwarz, J. P., Sodemann, H., Spackman, J. R., and Stohl, A.: An important contribution to springtime Arctic aerosol from biomass burning in Russia, Geophys. Res. Lett., 37, L01801,doi:10.1029/2009GL041816, 2010.
Watts, S. F.: The mass budget of carbonyl sulfide, dimethyl sulfide, carbon disulfide, and hydrogen sulfide, Atmos. Environ., 34, 761–779, 2000.
Wotton, B. M., Nock, C. A., and Flannigan, M. D.: Forest fire occurrence and climate change in Canada, Int. J. Wildland Fire, 19(3), 253–271, 2010.
Xiao, Y., Logan, J. A., Jacob, D. J., Hudman, R. C., Yantosca, R., and Blake, D. R.: Global budget of ethane and regional constraints on U. S. sources, J. Geophys. Res., 113, D21306, doi:10.1029/2007JD009415, 2008.

ACPD
11, 5435–5491, 2011

Table 1. WRF physics options used in this study. See Skamarock et al. (2008) for details about each option.

Option	Setting
Microphysics	Morrison Double-Moment
Longwave radiation	Rapid Radiative Transfer Model
Shortwave radiation	Goddard
Surface layer	ETA Similarity
Land surface	NOAH
Boundary layer	Mellor-Yamada-Janjic
Cumulus parameterization	Kain-Fritsch

ACPD
11, 5435–5491, 2011

Table 2. Atmospheric lifetime, analytical details, and measurement statistics for selected compounds measured in the Asian plume. ARCTAS-A background averages also are included.

Compound	Formula	Life-time	LOD (pptv)	Preci-sion (%)	Accu-racy (%)	Bkgd. Avg (pptv)	Bkgd. St. Dev. (pptv)	Asian Plume Avg. (pptv)	Asian Plume St. Dev. (pptv)	Enhancement over average background (%)	Asian Plume Max (pptv)
1,2-Dichloroethane	$C_2H_4Cl_2$	1–2 mo	0.1	5	10	11.0	0.8	57	9	420	64
Methyl chloride	CH_3Cl	1.0 yr	50	5	10	567	7	739	19	30	751
Halon-1211	$CBrClF_2$	16 yr	0.1	1	5	4.20	0.04	4.49	0.06	7	4.55
Carbonyl sulphide	OCS	2.5 yr	10	2	10	487	4	615	16	26	629
Tetrachloroethene	C_2Cl_4	2–3 mo	0.01	5	10	4.20	0.60	6.77	0.35	61	6.99
HCFC-22	CHF_2Cl	12 yr	2	5	5	195	2	211.3	1.0	8	212.3

ACPD
11, 5435–5491, 2011

Table 3. As in Table 2, but for the North American plume.

Compound	Formula	Life-time	LOD (pptv)	Preci-sion (%)	Accu-racy (%)	Bkgd. Avg (pptv)	Bkgd. St. Dev. (pptv)	North Ameri-can Plume Avg. (pptv)	North Ameri-can Plume St. Dev. (pptv)	Enhancement over average background (%)	North Ameri-can Plume Max (pptv)
Ethane	C_2H_6	47 d	3	1	5	1408	166	1932	225	37	2317
Propane	C_3H_8	11 d	3	2	5	312	59	573	122	83	798
Benzene	C_6H_6	9 d	3	3	5	49	12	86	13	76	103
HCFC-22	CHF_2Cl	12 yr	2	5	5	195	2	201	4	3	210
Tetrachloroethene	C_2Cl_4	2–3 mo	0.01	5	10	4.20	0.60	6.35	1.36	51	8.29

ACPD
11, 5435–5491, 2011

Table 4. As in Table 2, but for the European plume. Asterisks for CH_4 denote that its units are ppbv instead of pptv.

Compound	Formula	Life-time	LOD (pptv)	Preci-sion (%)	Accu-racy (%)	Bkgd. Avg (pptv)	Bkgd. St. Dev. (pptv)	European Plume Avg. (pptv)	European Plume St. Dev. (pptv)	Enhancement over average background (%)	European Plume Max (pptv)
Tetrachloroethene	C_2Cl_4	2–3 mo	0.01	5	10	4.20	0.60	6.03	0.86	44	6.93
Ethyne	C_2H_2	12–17 d	3	3	5	264	42	519	79	97	600
Benzene	C_6H_6	9 d	3	3	5	49	12	112	17	129	131
Methane (ppbv)	CH_4	9 yr	n/a	0.1	1	1840*	8*	1871*	8*	2	1877*
Ethane	C_2H_6	47 d	3	1	5	1408	166	1917	47	36	1972
Propane	C_3H_8	11 d	3	2	5	312	59	537	36	72	577

ACPD
11, 5435–5491, 2011

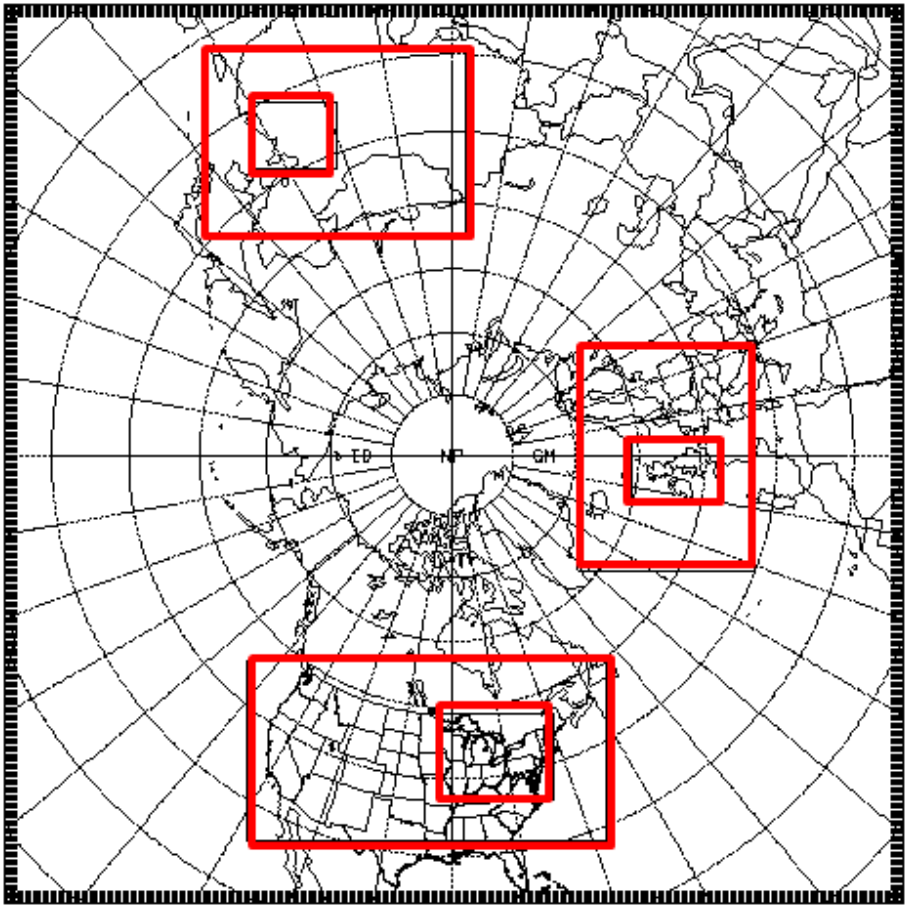

Fig. 1. Parent domain (45 km, black) and inner nests (15 km and 5 km, red) used for the ARCTAS simulations.

ACPD
11, 5435–5491, 2011

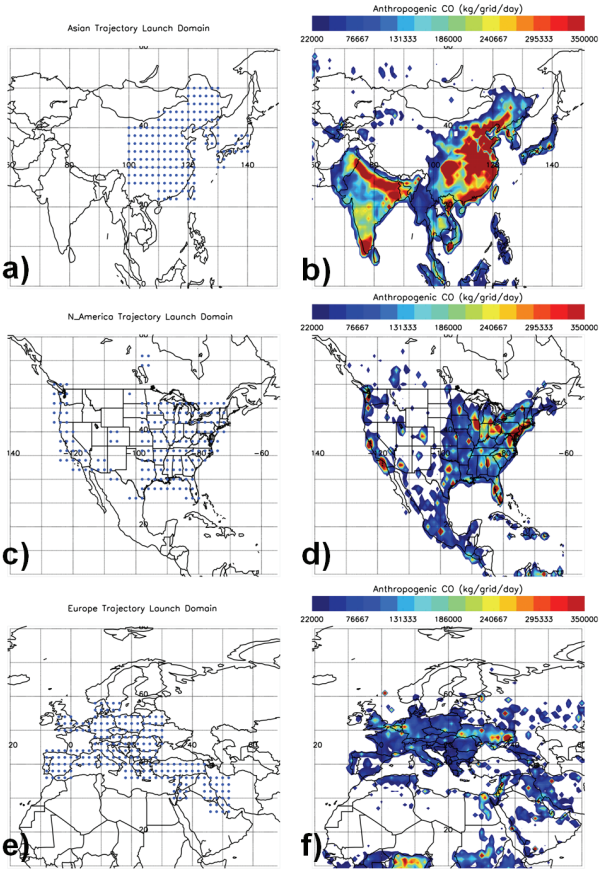

Fig. 2. Trajectory release locations on the 2.0°×2.0° grid (blue dots) for **(a)** Asia, **(c)** North America, and **(e)** Europe. These locations were based on anthropogenic emissions during ARCTAS (kg grid point^{-1} day^{-1}) for **(b)** Asia, **(d)** North America, and **(f)** Europe from the CGRER data set.

ACPD
11, 5435–5491, 2011

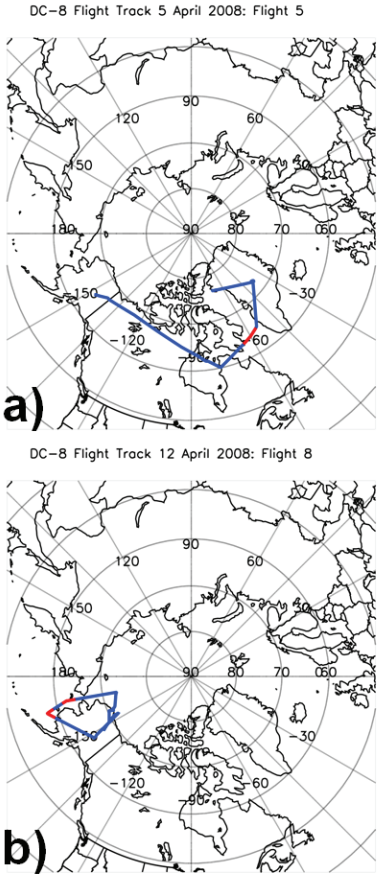

Fig. 3. DC-8 flight tracks for **(a)** flight 5 on 5 April 2008, and **(b)** flight 8 on 12 April 2008. Trajectories were released at 1 min intervals along the red segments.

ACPD
11, 5435–5491, 2011

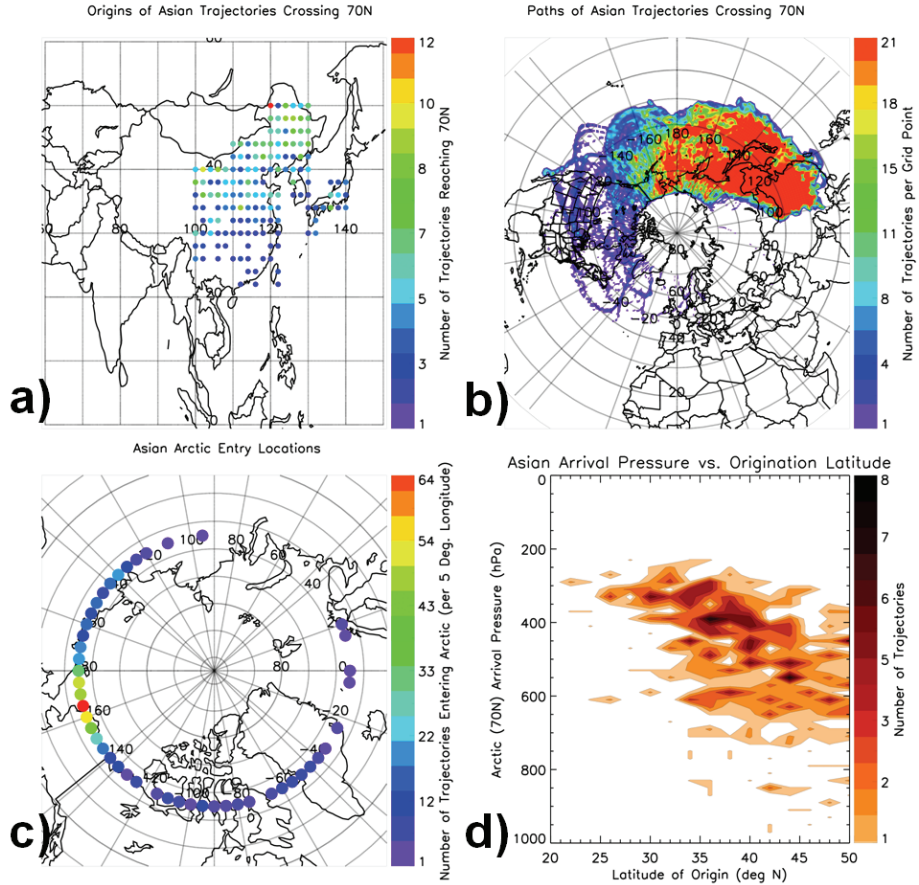

Fig. 4. Trajectory statistics for the Eastern Asia domain. **(a)** Number and originating locations of trajectories reaching the Arctic (70° N) within 15 days. **(b)** Pathways taken by all 15 day trajectories reaching the Arctic. **(c)** Number and location of trajectories entering the Arctic. **(d)** Pressure level at which Arctic bound trajectories arrive at 70° N.

ACPD
11, 5435–5491, 2011

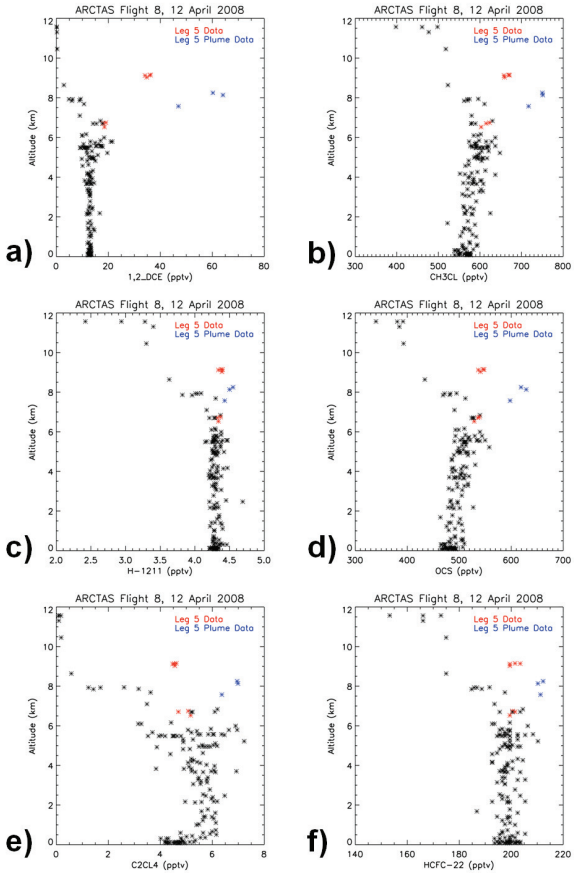

Fig. 5. Vertical distributions of data from flight 8 on 12 April 2008 for **(a)** 1,2-DCE, **(b)** CH_3Cl, **(c)** H-1211, **(d)** OCS, **(e)** C_2Cl_4, and **(f)** HCFC-22. Red points are data from leg 5. Blue points also are from leg 5 but represent the sampled plume. Black points represent the remaining legs of flight 8.

ACPD
11, 5435–5491, 2011

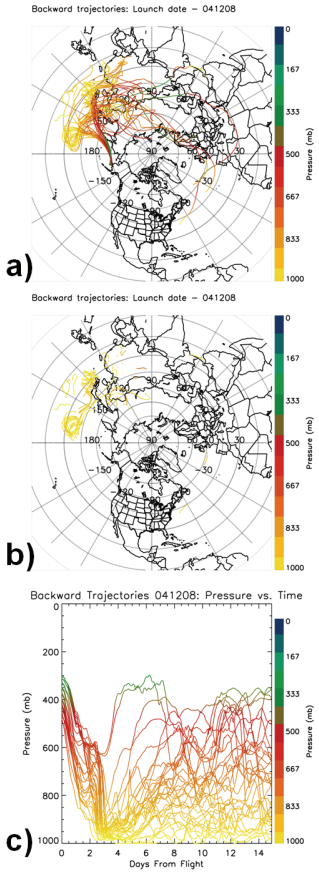

Fig. 6. Fifteen day backward trajectories for **(a)** all trajectories associated with leg 5 that encountered the boundary layer sometime during their 15 day transit, **(b)** only those segments of trajectories in **(a)** when the boundary layer is experienced, and **(c)** pressure vs. time plot for trajectories from leg 5 that encountered the boundary layer.

ACPD
11, 5435–5491, 2011

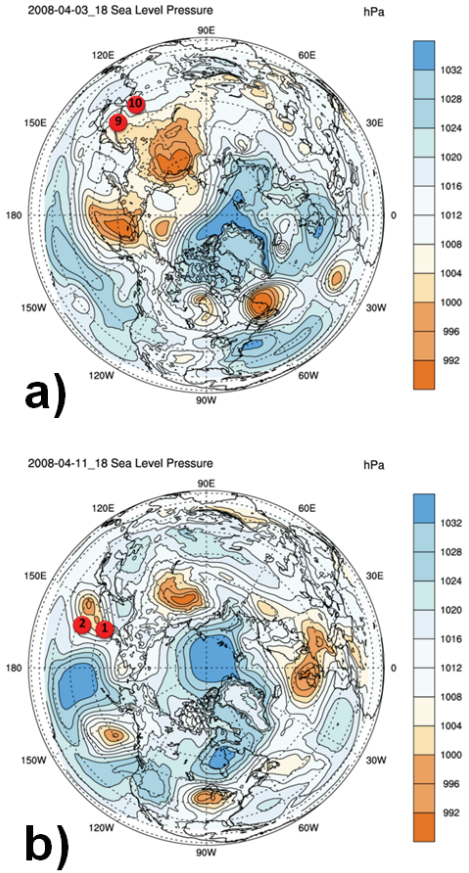

Fig. 7. Average location of trajectories comprising the easternmost branch in Fig. 6a (red circles) for **(a)** 9–10 days back from the flight, and **(b)** 1–2 days back.

ACPD
11, 5435–5491, 2011

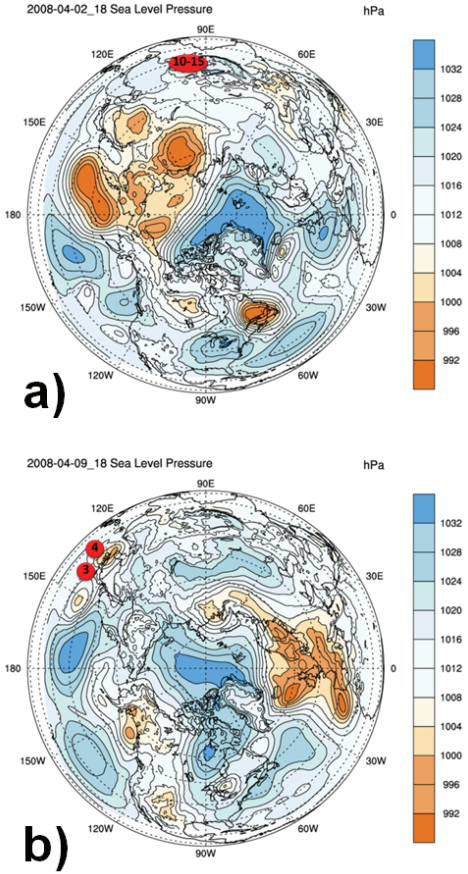

Fig. 8. Average location of trajectories comprising the westernmost branch in Fig. 6a (red circles) for **(a)** 10–15 days back from the flight, and **(b)** 3–4 days back.

ACPD
11, 5435–5491, 2011

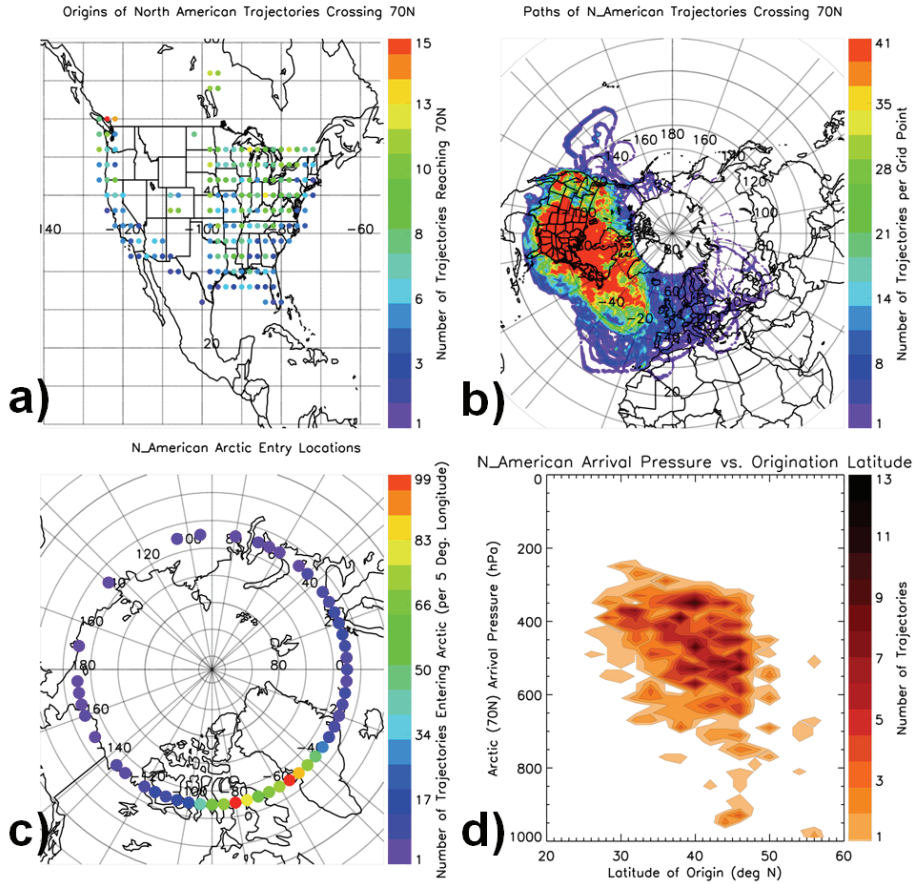

Fig. 9. As in Fig. 4, but for North American trajectories.

ACPD
11, 5435–5491, 2011

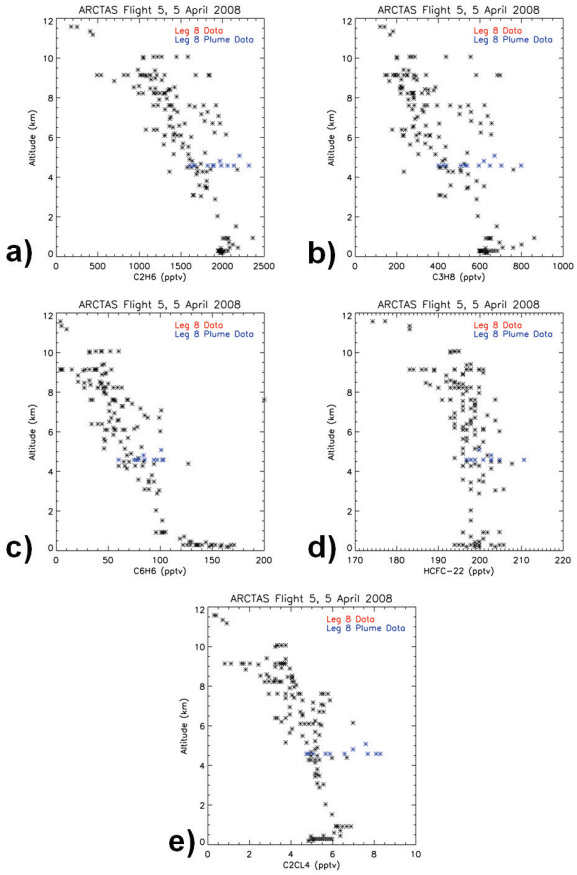

Fig. 10. Vertical distributions of data from flight 5 on 5 April 2008 for **(a)** C_2H_6, **(b)** C_3H_8, **(c)** C_6H_6, **(d)** HCFC-22, and **(e)** C_2Cl_4. Blue points are from leg 8, representing the sampled plume. In this case the plume is represented by all of the data points along leg 8. Black points represent the remaining legs of flight 5.

ACPD
11, 5435–5491, 2011

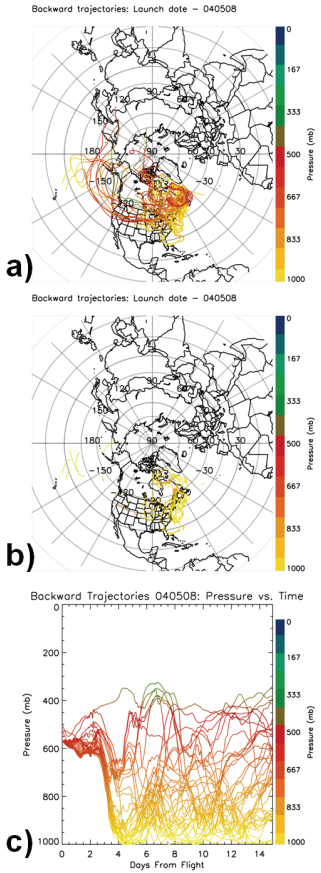

Fig. 11. As in Fig. 6, but for leg 8 on 5 April 2008.

ACPD
11, 5435–5491, 2011

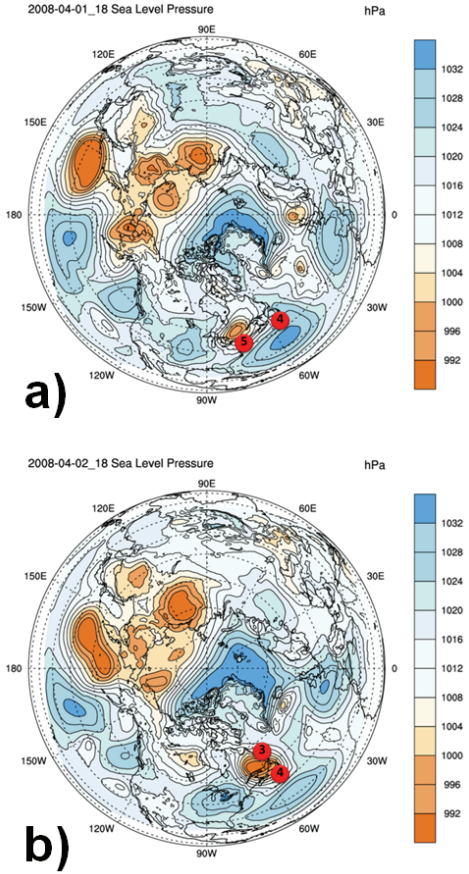

Fig. 12. Average positions of the group of trajectories released from leg 8 of DC-8 flight 5 on 5 April 2008. Red circles denote locations at **(a)** 4–5 days back and **(b)** 3–4 days back.

ACPD
11, 5435–5491, 2011

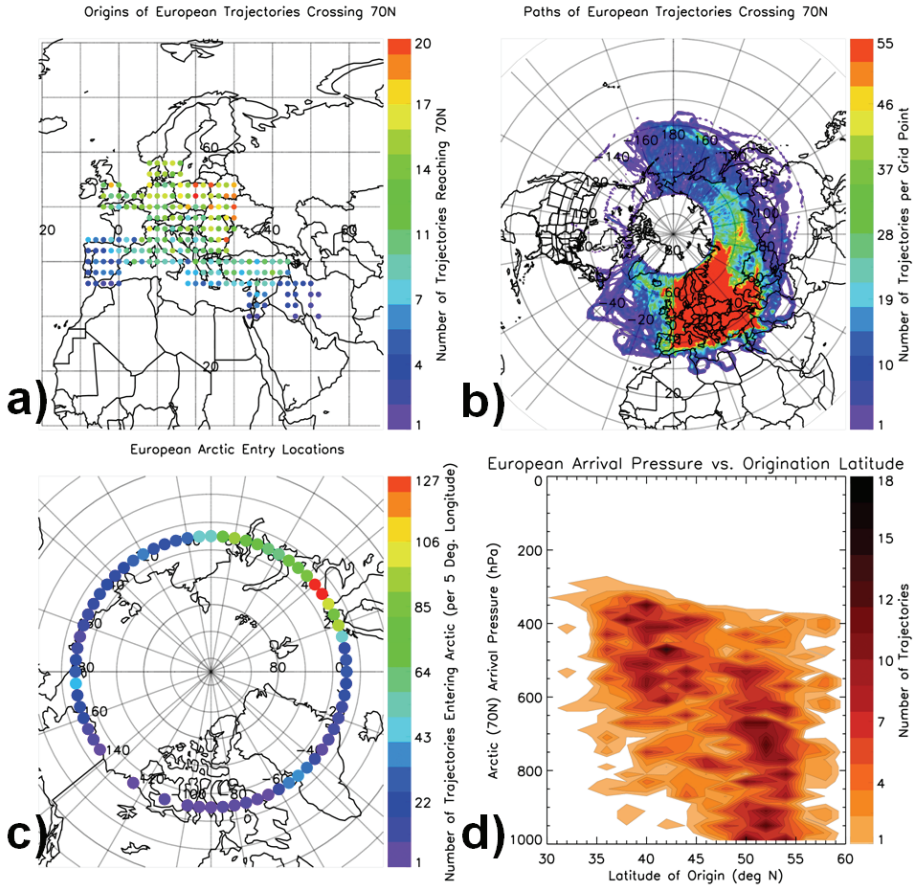

Fig. 13. As in Fig. 4, but for trajectories released from areas of European anthropogenic emissions.

ACPD
11, 5435–5491, 2011

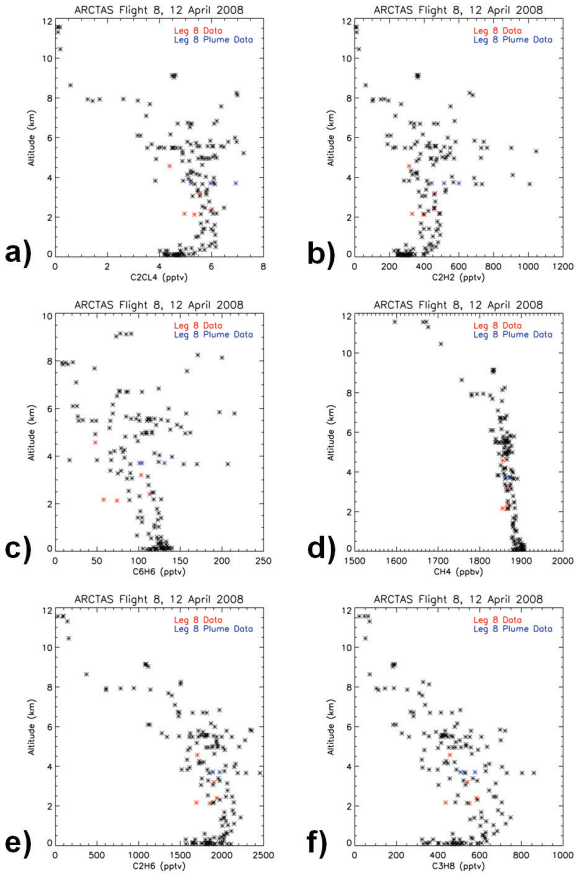

Fig. 14. Vertical distributions of data from flight 8 on 12 April 2008 for **(a)** C_2Cl_4, **(b)** C_2H_2, **(c)** C_6H_6, **(d)** CH_4, **(e)** C_2H_6, and **(f)** C_3H_8. Red points are data from leg 8. Blue points also are from leg 8 but represent the sampled plume. Black points represent the remaining legs of flight 8.

ACPD
11, 5435–5491, 2011

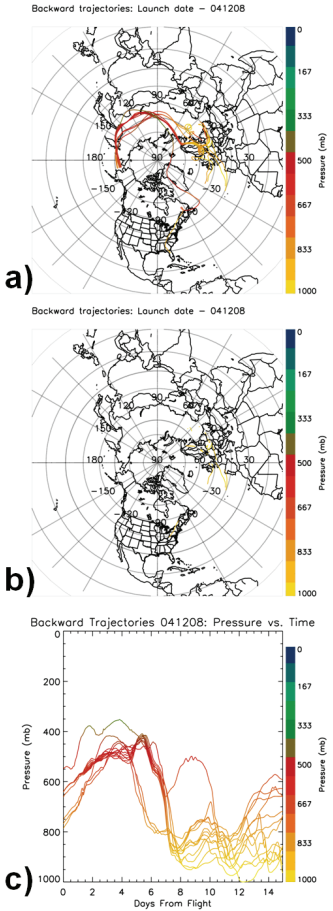

Fig. 15. As in Fig. 6, but for leg 8 on 12 April 2008.

ACPD
11, 5435–5491, 2011

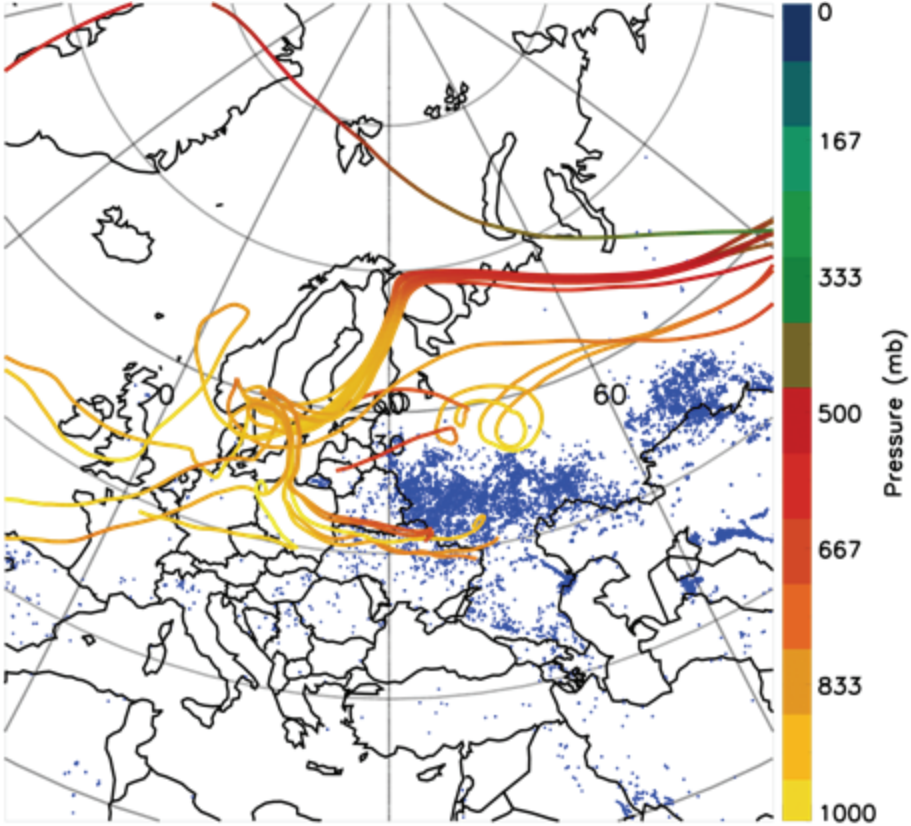

Fig. 16. Trajectories as in Fig. 15a plotted with FLAMBE data (blue dots) for the period 26 March–6 April 2008.

ACPD
11, 5435–5491, 2011

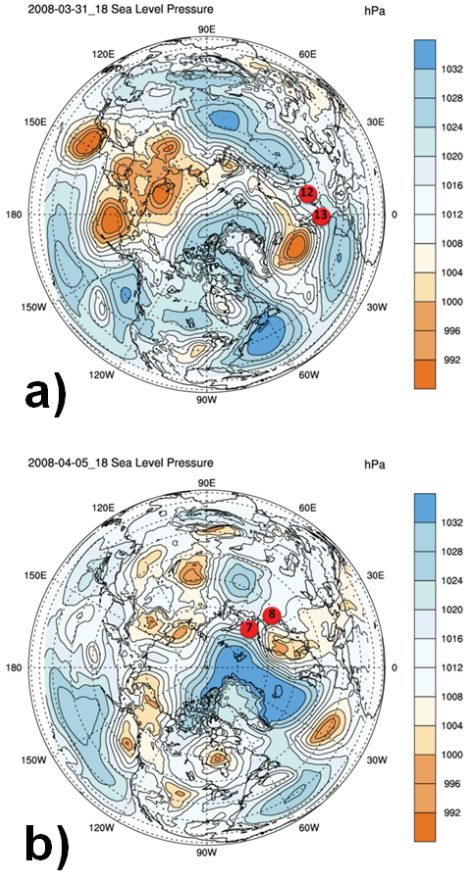

Fig. 17. Average location of trajectories comprising the largest group of trajectories in Fig. 15a (red circles) for **(a)** 12–13 days back from the flight and **(b)** 7–8 days back.

ACPD
11, 5435–5491, 2011